



Skill assessment of global climate model wind speed from CMIP5 and CMIP6 and evaluation of projections for the Bay of Bengal

Athira Krishnan¹ · Prasad K. Bhaskaran¹

Received: 14 May 2020 / Accepted: 29 July 2020 / Published online: 3 August 2020
© Springer-Verlag GmbH Germany, part of Springer Nature 2020

Abstract

Atmospheric and oceanic parameters derived from global climate model (GCM) simulations have received wide global attention and importance in representing the future world under different scenarios of greenhouse gas emissions. The present study deals with near-surface wind speed in the Bay of Bengal (BoB) obtained from CMIP5 and the upcoming CMIP6 GCMs and validation exercise clearly signify improved performance of CMIP6 GCMs over CMIP5. Multi-model ensemble mean corresponding to the four emission scenarios are constructed using the best performing models of CMIP6 family. The study reveals that near-future changes in wind speed in the BoB are moderate under the low-end scenario of SSP1-2.6. Projected wind speeds in the head BoB are expected to increase or decrease by 20% during June–July–August and December–January–February under high-end scenario by the end of twenty-first century. A positive change up to 30% in the northeast monsoon winds under SSP5-8.5 is projected in the central BoB. Irrespective of the seasons, a net increase amounting to 0.6–0.8 m/s is observed along the east coast of India under SSP2-4.5 scenario by the mid and end of the century. Maximum rise by 25% (0.5–1 m/s) in wind speed is predicted under SSP3-7.0 scenario in the near future. Further, the study points out a decline in wind speed by 0.2–0.8 m/s in the central and southern BoB under the extreme scenario of SSP5-8.5. Strengthening and weakening of winds over the BoB accounts the projected variations in temperature that resulted from global warming and subsequent changes in atmospheric circulation.

Keywords CMIP5 · CMIP6 · GCMs · SSPs · Wind speed · Bay of Bengal

1 Introduction

The Indian Ocean during the past half century has been warming throughout, and there are few case studies that investigated the cause and effect of basin-scale Indian Ocean warming (Klein et al. 1999; Dong et al. 2014; Swapna et al. 2014). Studies based on analysis of sea surface temperature (SST) indicates that the western Indian Ocean has been undergoing warming for over a century (Roxy et al. 2014). The rise in SST evokes manifold effects such as changes in surface pressure distribution leading to varying wind patterns, sea-level rise, and other consequences. Understanding the variability in wind speed have many practical implications such as the estimation of wind power potential of any

given geographical region and also to develop future wind-wave climate projections for planning of coastal activities, coastal zone management, etc. Influence of climate change on wind and wave characteristics are discussed in few studies (Kumar et al. (2016); Semedo et al. 2011, 2013; Wang et al. 2014; Reguero et al. 2012; Young and Ribal 2019). There are only handful of studies attempted so far to understand the wind speed distribution and its variability over the global oceans. The mean wind speeds over the global oceans have increased by 0.25–0.5% per year (Young et al. 2011) and at a rate of 0.080 m/s/decade (Wentz et al. 2007). Near-surface wind speed showed a declining trend of 0.140 m/s/decade (McVicar et al. 2012), 0.084 m/s/decade from wave- and anemometer-based sea surface wind (WASWind) dataset and 0.134 m/s/decade using special sensor microwave imagers (SSM/Is) (Tokinaga and Xie 2011). In context to the Indian Ocean (IO), there are limited studies available that are recognized for its peculiar behaviour in wind climate (Nayak et al. 2013; Sandhya et al. 2013; Bhaskaran et al. 2014; Gupta et al. 2015, 2017; Gupta and Bhaskaran 2016;

✉ Prasad K. Bhaskaran
prasadsu@yahoo.com; pkbhaskaran@naval.iitkgp.ac.in

¹ Department of Ocean Engineering and Naval Architecture, Indian Institute of Technology Kharagpur, Kharagpur, West Bengal 721 302, India

Parvathy and Bhaskaran 2019; Bhaskaran 2019; Patra and Bhaskaran 2016; Abram et al. 2020; Kumar et al. 2019). The reality behind the increase or decrease in wind speed is directly affected by the external factors (greenhouse gases, aerosols, solar output, etc.), and the expected variability in the future is probabilistic.

The past, present, and future scenarios of climate change are brought out for the scientific community by the World Climate Research Programme (WCRP) under the Intergovernmental Panel on climate change (IPCC). The group of climate models developed under this program convey crucial information about the earth system and also provide projections of probabilistic scenarios of futuristic change dealing with sustainable pathways to unsustainable growth. The 3rd and 5th phases of Coupled Model Inter-comparison Project (CMIP) models are being widely used by the scientific community worldwide in various disciplines. These models also provide essential information on futuristic projections of wind speed over the Indian Ocean. Further, the global climate models (GCMs) under the CMIP family also provide scenarios for different representative concentration pathways (RCPs) keeping in view the inherent uncertainties involved in the greenhouse gas emissions. Stable wind and wave climate projections for IO are brought out by Kamranzad and Mori (2019) employing super-high-resolution model MRI-AGCM3.2S under the RCP 8.5 scenario. Over the AS, CMIP5 models reveal a weakening of winter monsoon winds ranging between 3.5 and 6.5% for RCP 4.5 and RCP 8.5. Warming of the dry Arabian Peninsula, resulting in a decline of inter-hemispheric sea level pressure gradient attributes to the reason behind the weakening of winds (Parvathi et al. 2017). They also observed that projected winter surface winds under RCP 8.5 weaken over most of the Indian Ocean regions with exception for BoB. Head BoB region showed an increase of 2% under the RCP 8.5 scenario, on the other hand, central BoB exhibited a marginal rise in wind speed under both RCP 4.5 and 8.5 scenarios by the end of the century. In addition, the mean wind speed during the mid-century has declined by 0.25 to 0.5 m/s and 0.3–0.5 m/s under RCP 4.5 and 8.5 scenarios, respectively (Mohan and Bhaskaran 2019b). Comparison of wind speed simulated by CMIP5 models against reanalysis products, satellite data, and in-situ observations resulted in converging to the best performing models, which in turn was used as a tool for projecting future with better accuracy (Krishnan and Bhaskaran 2019a, b).

Uncertainties in simulating the climate systems appear as biases in the results obtained from the climate model run. Lee et al. (2013) reported that the magnitude of seasonal variability in wind stress averaged over global oceans are overestimated by almost 50% in the CMIP models. Bias error up to 4 m/s was noticed for the BoB domain (Krishnan and Bhaskaran 2019b) when compared against altimeter

data. North Indian Ocean showed a bias of 1–2 m/s for wind speed estimated from the ensemble mean of models (Mohan and Bhaskaran 2019a). A very recent study by Morim et al. (2020) reported that historical wind speeds simulated by CMIP5 models propagate uncertainty within the ensemble having strong latitudinal dependence and thereby produce large-scale spatial patterns in wind speed. Variations in the representation of mesoscale and sub-mesoscale processes caused by coarse grid resolutions in GCMs might affect the projected values of wind speed data. In addition, future projections in the RCP scenarios developed under the CMIP5 project does not account for the future land-use-land-cover (LULC) changes (Kulkarni and Huang 2014). Furthermore, the bias in the model outputs result due to the lack of flux corrections between the atmosphere and ocean (Muthige et al. 2018). Especially the biases in simulating wind speeds are related to the underlying physics of the atmospheric component in the models (Morim et al. 2020).

Understanding the shortcomings of CMIP5, the upcoming IPCC 6th Assessment Report is releasing a set of GCMs under the CMIP6 project. According to Eyring et al. (2016) and Stouffer et al. (2017), various advancements and efforts have taken place to develop a new set of models under CMIP6. They are enlisted as identification of model errors, a modified estimate of future projections, accounting for responses to aerosols and short-term forcing agents, advanced study on decadal climate variability, and to fill the other scientific gaps of CMIP5 phase. While CMIP5 discussed projections under different RCPs (2.6, 4.5, 6.0, and 8.5), the CMIP6 project brings out various shared socio-economic pathways (SSP) ranging from 1.9 to 8.5 W/m² projected for end of the century. These SSPs standardizes all socio-economic assumptions, i.e., population, GDP, poverty which helps to analyze the expected climate outcomes under each of the pathways (Gidden et al. 2019). A detailed evaluation and skill assessment on the performance of different GCMs developed under the CMIP6 project in simulating wind speed is an essential pre-requisite to better represent the projections. Therefore, our study performed a comprehensive assessment based on inter-comparison experiments between CMIP5 and CMIP6 models facilitating the wind climate projections for BoB region having practical relevance. The analysis involves a detailed examination of historical data simulated by both CMIP5 and CMIP6 models validated against available in situ data. Further the study summarizes on the projected scenarios utilizing the CMIP6 product. The paper is organized as follows: Sect. 2 and 3 deals with the data and diagnostic parameters, and methodology used in the present study. The results and discussion are dealt in Sect. 4 covering aspects on critical assessment of global climate model wind speeds from CMIP5 and CMIP6 and evaluation of projections for the BoB region. Finally, the Sect. 5 deals with the overall conclusions obtained from this study.

2 Data

Best performing climate models under the CMIP5 category (<https://esgf-node.llnl.gov/projects/cmip5/>) verified for the BoB region (Table 1) and reported by Krishnan and Bhaskaran (2019a, b) are employed in the current study. The available 20 GCMs (<https://esgf-node.llnl.gov/search/cmip6/>) under CMIP6 are being considered for performance evaluation (Table 2). The models employed for the present study under CMIP5 and CMIP6 belongs to ensemble ‘r1i1p1’ and ‘r1i1p1f1’ respectively. The monthly near-surface wind speed data simulated by GCMs are extracted for the historical and projection analysis. Four SSP scenarios under the Tier-1 experiment such as SSP1-2.6, SSP2-4.5, SSP3-7.0, and SSP5-8.5 are considered for evaluating the future changes in wind speed. These emission scenarios corresponds to the low-end future category indicating the end-century temperature rise to be less than 2° to a high-end future with a temperature rise of 5° (Gidden et al. 2019). More details on the different SSP scenarios are presented in Table 3.

The skill level of simulated near-surface wind speed from models under the CMIP5 and CMIP6 family are evaluated against merged scatterometer data (Sreelakshmi and Bhaskaran 2020) the ERA-interim Reanalysis product, and in-situ observations from Research Moored Array for African–Asian–Australian Monsoon Analysis and Prediction (RAMA) buoys (Table 4). Satellite scatterometer missions like ERS-1/2, QuikSCAT, and ASCAT together provide

near-surface wind speed information for the period from 1992 to 2014 (<https://apdr.c.soest.hawaii.edu/data/data.php>). Wind speed data having spatial resolution of 100 km retrieved from ERS-1/2 missions are widely validated and also used for different applications (Lehner et al. 2000; Vandemark et al. 1998; Hasager et al. 2004). Wind vectors at a resolution of 25 km from QuikSCAT were used for many studies globally (Sempreviva et al. 2006; Chu et al. 2004; Ebuchi et al. 2002; Bentamy and Denis 2012). Gridded data products of ASCAT are available at 0.25° resolutions and highly recommended for meteorological applications as they are claimed to be good in wind retrievals during rain, high winds, and tropical cyclones (Figsaldaña et al. 2002; Bentamy et al. 2008; Rani et al. 2014). Monthly wind speed data retrieved from these satellites, ERS-1 (1992–1996), ERS-2 (1997–1999), QuikSCAT (1999–2007), ASCAT (2008–2014) are merged to form a continuous time series of 23 years and used as primary reference dataset in the study. In addition, this study also performed an inter-comparison exercise utilizing the reanalysis product ERA-interim developed by European Centre for Medium-Range Weather Forecasts (ECMWF, Dee et al. 2011) (<https://apps.ecmwf.int/datasets/data/interim-full-daily/levtype=sfc/>). ERA-interim products are widely used as they are available at different temporal and spatial resolutions, and have proven to perform well for various wind speed applications (Patra and Bhaskaran 2016; Carvalho et al. 2014a, b; Nagababu et al. 2017).

ERA-interim incorporates the blend of data from various sources such as satellite, in situ (buoys, radiosondes,

Table 1 List of various CMIP5 models used for the study (Source URL: <https://portal.enes.org/data/enes-model-data/cmip5/resolution>)

Sl. No.	Model ID/acronym	Expansion	Spatial resolution (in °)
1	CanESM2	Canadian Centre for Climate Modelling and Analysis, Canada	2.81×2.79
2	CMCC-CM	Centro Euro-Mediterraneo per I Cambiamenti Climatici, Italy	0.75×0.75
3	CNRM-CM5	Centre National de Recherches Meteorologiques/Centre Europeen de Recherche et Formation Avancees en Calcul Scientifique, France	1.41×1.40
4	ACCESS1.0	CSIRO (Commonwealth Scientific and Industrial Research Organisation, Australia), and BOM (Bureau of Meteorology, Australia)	1.87×1.25
5	ACCESS1.3		
6	HadGEM2-ES	Met Office Hadley Centre (additional HadGEM2-ES realisations contributed by Instituto Nacional de Pesquisas Espaciais), U.K	1.87×1.25
7	MPI-ESM-LR	Max Planck Institute for Meteorology (MPI-M), Germany	1.87×1.85
8	MPI-ESM-MR		
9	GISS-E2-H	NASA Goddard Institute for Space Studies, USA	2.00×2.50
10	GISS-E2-H-CC		
11	GISS-E2-R		
12	GISS-E2-R-CC		
13	HadGEM2-AO	National Institute of Meteorological Research/Korea Meteorological Administration, Korea	1.25×1.87
14	MIROC5	Atmosphere and Ocean Research Institute (The University of Tokyo), National Institute for Environmental Studies, and Japan Agency for Marine–Earth Science and Technology, Japan	1.41×1.39

Table 2 List of various CMIP6 models used for the study (Source URL: https://wcrp-cmip.github.io/CMIP6_CVs/docs/CMIP6_source_id.html)

Sl. nso.	Model name/acronym	Institute	Resolution (km)
1	MRI-ESM2-0	Meteorological Research Institute-Earth System Model, Japan	100
2	CESM2	National Center for Atmospheric Research-Community Earth System Model, USA	100
3	CESM2-WACCM	National Center for Atmospheric Research. Community Earth System Model-Whole Atmosphere Community Climate Model, USA	100
4	BCC-CSM2-MR	Beijing Climate Center climate system model version 2, China	100
5	SAM0-UNICON	Seoul National University Atmosphere Model version 0 with a Unified Convection Scheme, Korea	100
6	MIROC6	Model for Interdisciplinary Research on Climate, University of Tokyo, NIES, and JAMSTEC, Japan	250
7	BCC-ESM1	Beijing Climate Center Earth system model, China	250
8	GISS-E2-1-G	National Aeronautics and Space Administration. Goddard Institute for Space Studies-Model E Version 2, USA	250
9	GISS-E2-1-H	National Aeronautics and Space Administration. Goddard Institute for Space Studies-Model E Version 2-Hycom Ocean Model, USA	250
10	CanESM5	Canadian Centre for Climate modelling and analysis. Canadian Earth system model, Canada	500
11	E3SM-1-0	Energy Exa-scale Earth System Model, U.S. Department of Energy	100
12	EC-Earth3	European Centre of Medium Range Weather Forecast, UK	100
13	FGOALS-f3-L	Flexible Global Ocean–Atmosphere–Land System, Chinese Academy of Sciences (CAS)	100
14	FGOALS-g3	Flexible Global Ocean–Atmosphere–Land System model, Grid-point Version 3, Chinese Academy of Sciences (CAS)	250
15	GFDL-CM4	Coupled Physical Model, CM4, Geophysical Fluid Dynamics Laboratory, USA	100
16	GFDL-ESM4	Earth System (ESM4), Geophysical Fluid Dynamics Laboratory, USA	100
17	GISS-E2-1-G-CC	National Aeronautics and Space Administration. Goddard Institute for Space Studies-Model E Version 2, USA	250
18	IPSL-CM6A-LR	Institut Pierre Simon Laplace, Paris 75,252, France (IPSL)	50
19	MPI-ESM1-2-h	Max Planck Institute Earth System Model, HR, Germany	100
20	NorCPM1	Norwegian Climate Prediction Model, Norway	250

Table 3 Overview of the shared Socio-economic pathways (SSPs) (from Gidden et al. 2019)

Emission scenario	Scenario description
SSP1-2.6	Strong economic growth via sustainable pathways
SSP2-4.5	Middle of-the-road scenario with moderate population growth and slower convergence of income levels across countries Intermediate vulnerability and climate forcing and its median positioning of land use and aerosol emissions
SSP3-7.0	Futures with high inequality between countries (i.e., “regional rivalry”) and within countries Quantification of avoided impacts (e.g., relative to SSP2) and has significant emissions from near-term climate forcing (NTCF) species such as aerosols and methane (also referred to as short-lived climate forcers, or SLCHF)
SSP5-8.5	Strong economic growth via fossil fuel pathways, delayed climate action End of the century (EOC) temperature outcomes span a large range, from 1.4 °C at the lower-end to 4.9 °C for SSP5-8.5

pilot balloons, aircraft, and wind profilers) and model simulations in the data assimilation procedure and produces long-term global data which makes it widely applicable in the field of climate research (Brower et al. 2013; Carvalho et al. 2017; Simmons et al. 2017; Lee et al. 2013; Zou and Kaminski 2014). ERA-interim data is also employed as official validation dataset for CMIP5 model downscaling experiment, CORDEX initiative (Brands et al. 2013). In situ observations by buoys are considered to be superior among reference datasets (Satellite

retrievals, Reanalysis products, ship borne data and buoy observation) for model validations. Hence, validation is also performed using wind speed obtained from RAMA buoys, the observational array network in central BoB region designed to understand the Indian Ocean variability and the monsoon (McPhaden et al. 2009). The best performing models were selected based on model performance against the three reference datasets. More details on the datasets used in the present study are shown in Tables 1, 2, 3, 4.

Table 4 Details of the datasets used in the study

Sl. no.	Data	Temporal resolution	Spatial resolution	Time period
1	CMIP5 (14 Models)	Monthly	Varies	Jan 1992–Dec 2005 (Historical)
2	CMIP6 (20 Models)	Monthly	Varies	Jan 1992–Dec 2014 (Historical) Jan 2015–Dec 2100 (Projection)
3	ERA-interim	Monthly	1° × 1°	Jan 1992–Dec 2014
4	ERS-1	Monthly	0.5° × 0.5°	Jan 1992–Mar 1996
5	ERS-2	Monthly	0.5° × 0.5°	Apr 1996–July 1999
6	QuikSCAT	Monthly	0.25° × 0.25°	Aug 1999–Dec 2007
7	ASCAT	Daily	0.25° × 0.25°	Jan 2008–Dec 2014
8	RAMA Buoys	Monthly	8° N 90° E 12° N 90° E 15° N 90° E	2008, 2011, 2012 2010, 2013, 2014 2009

3 Methods

Statistical evaluation of climate models are performed using the Taylor Diagram (Taylor 2001). It is an advanced method to express the skill level of models by representing the correlation coefficient (R), standard deviation, and root mean square error ($RMSE$) between the models and reference datasets (Lee et al. 2013). Historical data on wind speed are available till 2005 for CMIP5 and till 2014 for the CMIP6 project. For an inter-comparison exercise between CMIP5 and CMIP6 models, a common period of 1992–2005 is considered for both models as well the reference datasets. In order to facilitate the comparison, all datasets are interpolated to a horizontal grid size of 1° × 1° and with monthly intervals (Parvathi et al. 2017). To avoid the data gaps in coastal areas, the Taylor diagram considered only corresponding dataset of mean wind speed at each time step for the selected box (Fig. 1) in the central BoB region (84° E–90° E; 8° N–16° N). RAMA buoys located over the central BoB provides wind speed information at 4 m vertical height. They are scaled-up to the 10 m height using the logarithmic wind profile relation (Manwell et al. 2010; Krishnan and Bhaskaran 2019a).

$$\frac{U(z)}{U(Z_r)} = \frac{\ln\left(\frac{z}{z_0}\right)}{\ln\left(\frac{Z_r}{z_0}\right)} \quad (1)$$

where $U(z)$ represents the velocity to be estimated at a given vertical height Z above the mean level, $U(Z_r)$ represents the known velocity at a vertical level Z_r , the reference height where $U(Z_r)$ is known, and z_0 is the roughness length in the current wind direction (0.0002 for water surface).

Further, for evaluation purpose the wind speed from CMIP6 models are extracted at the in-situ RAMA buoy locations at corresponding time intervals. Comparison between models and RAMA is carried out by calculating various statistical quantities such as R , Bias error (B),

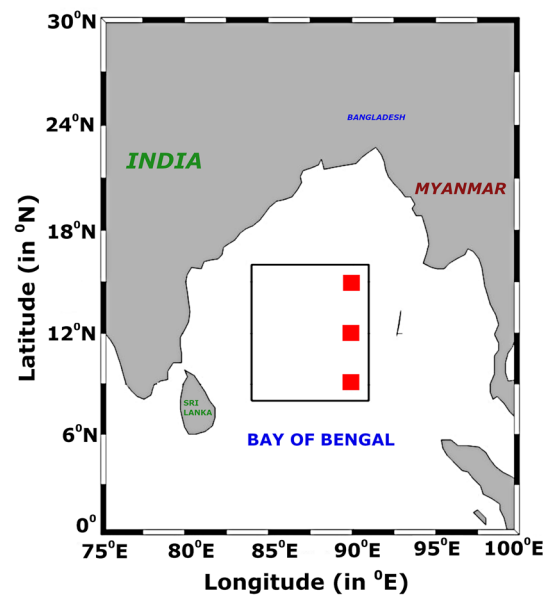


Fig. 1 Map of the study area (red dots indicate the location of RAMA buoys)

$RMSE$, Nash–Sutcliffe Efficiency (NSE ; Nash and Sutcliffe 1970) and Index of Agreement (IA ; Willmott et al. 1985). The performance score (PS) is defined as:

$$PS = 1 - \frac{(x_c - x_m)^2}{(x_m - x_R)^2} \quad (2)$$

where x_c denotes the computed or modeled values and x_m the measured or reference data. For the necessary condition, when x_R the reference value is the mean of measured data, then the PS becomes NSE . The NSE is a widely employed technique in the field of modelling to assess the predictive skill of models (Ghorbani et al. 2016; Lin et al. 2017). It can range between $-\infty$ and 1. For unbiased predictions,

the efficiency index lies within the interval from 0 to +1. However, for biased models the efficiency index may be algebraically negative. An *NSE* value close to 1 indicates a perfect match between modelled values and observations. An efficiency of zero indicates that the model predictions are very close to the mean of observed data, and efficiency less than zero ($NSE < 0$) occurs when the observed mean is a better predictor than the model. Threshold values that indicate model of sufficient quality have been suggested as $0.5 < NSE < 0.65$ (Ritter and Muñoz-Carpena 2013; Moriasi et al. 2007). The *IA* is defined as:

$$IA = \frac{(x_c - x_m)^2}{(|x_c - x_c| + |x_m - x_m|)^2} \tag{3}$$

The *IA* values close to 1 shows a better agreement between the predicted and measured values. Overall Performance Score interprets the model predictability by calculating residual error and the existing variability among the datasets. The magnitude of skill score value decides the performance of models with respect to observations, and more details on the performance score qualifications are provided in Table 5.

The drawbacks of a single model can be minimized by constructing the multi-model ensemble mean, and they are found to be far superior as compared to a single model (IPCC 2013). Based on the statistical analyses performed, the best performing models were selected and employed to construct a multi-model mean (MMM) to understand the future changes. Trend analysis was performed spatially over the study domain using the linear regression method, which estimates the rate of change of wind speed per year. Mann–Kendall (*MK*) test (Mann 1945; Kendall 1975) is a non-parametric test widely used to statistically assess the monotonic trends of data over time that computes the Mann–Kendall Tau, and Sen’s Slope. The *MK* test is quite popular and used in various fields across several disciplines (Crawford et al. 1983; Zhang et al. 2000; Rehman 2013; Birsan et al. 2013; Celik and Cengiz 2014; Gocic and Trajkovic 2013). The present study used the *MK* test to verify the significance level of trend in various datasets being used. The Sen’s slope value signifies an upward or downward trend of the variable over time. *MK* test at a 95% significance level

is performed to examine the trends in data along with Sen’s slope (Helsel and Hirsch 1992; Patra and Bhaskaran 2017).

Future changes in the wind speeds from CMIP5 ensemble for the near future (2026–2050), mid-century (2051–2075), and end-century (2076–2100) are calculated as the respective change from historical period (1980–2014). Percentage change in projected wind speed under different SSP scenarios are defined as (Mohan and Bhaskaran 2019b):

$$Futurechange = \left(\frac{Mean_{future} - Mean_{historical}}{Mean_{historical}} \right) \times 100 \tag{4}$$

Projected changes in wind speed distribution over the BoB region were calculated under the SSP scenarios of Tier-1 experiments. They show a wide range of future forcing scenarios which are, SSP1-2.6, SSP2-4.5, SSP3-7.0 and SSP5-8.5. The seasonal changes in wind speed for future were also obtained for the winter (December–January–February) and Summer (June–July–August) seasons (Rahaman et al. 2020).

4 Results and discussions

4.1 Inter-comparison of CMIP5 and CMIP6 models with reference datasets

A preliminary analysis by inter-comparison of various models under the CMIP5 and CMIP6 family was carried out by representing the statistical variables together in a Taylor diagram. Figure 2 shows the inter-comparison of wind speeds from CMIP5, CMIP6, ERA-interim, and scatterometer are chosen for a common time span of 1992–2005 representing the historical period. The Taylor skill of best-performing 14 GCMs participating CMIP5 from the previous studies (Krishnan and Bhaskaran 2019a, b) and 20 GCMs from CMIP6 are being used for the inter-comparison exercise. The best performing models selected from CMIP5 family represents the category having a good correlation of 0.7–0.9 and RMSE of 0.8–1.7 m/s when compared with ERA-interim and scatterometer data. However, a comparison with CMIP6 GCMs reveal that NorCPM1 is found to be the least correlated amongst the 20 models. The remaining models in CMIP6 family has a correlation ranging between 0.7 and 0.9 similar to CMIP5. The *R* obtained by comparing with scatterometer winds are relatively lower than that obtained by comparing with ERA-interim winds. It is noteworthy from the present comparison analysis that a greater number of CMIP6 models fit into correlation range of 0.8–0.9 and RMSE of 1.0–1.5 m/s than CMIP5 models. Also, there is a need to verify the expected improvements in the CMIP6 models as compared to CMIP5 models on spatial scales. Therefore, the best performing models from Taylor’s skill

Table 5 Performance Score (PS) qualifications (Source: <https://cirpwiki.info/wiki/Statistics>)

Range	Qualification
0.8 < PS < 1.0	Excellent
0.6 < PS < 0.8	Good
0.3 < PS < 0.6	Reasonable
0 < PS < 0.3	Poor
PS < 0	Bad

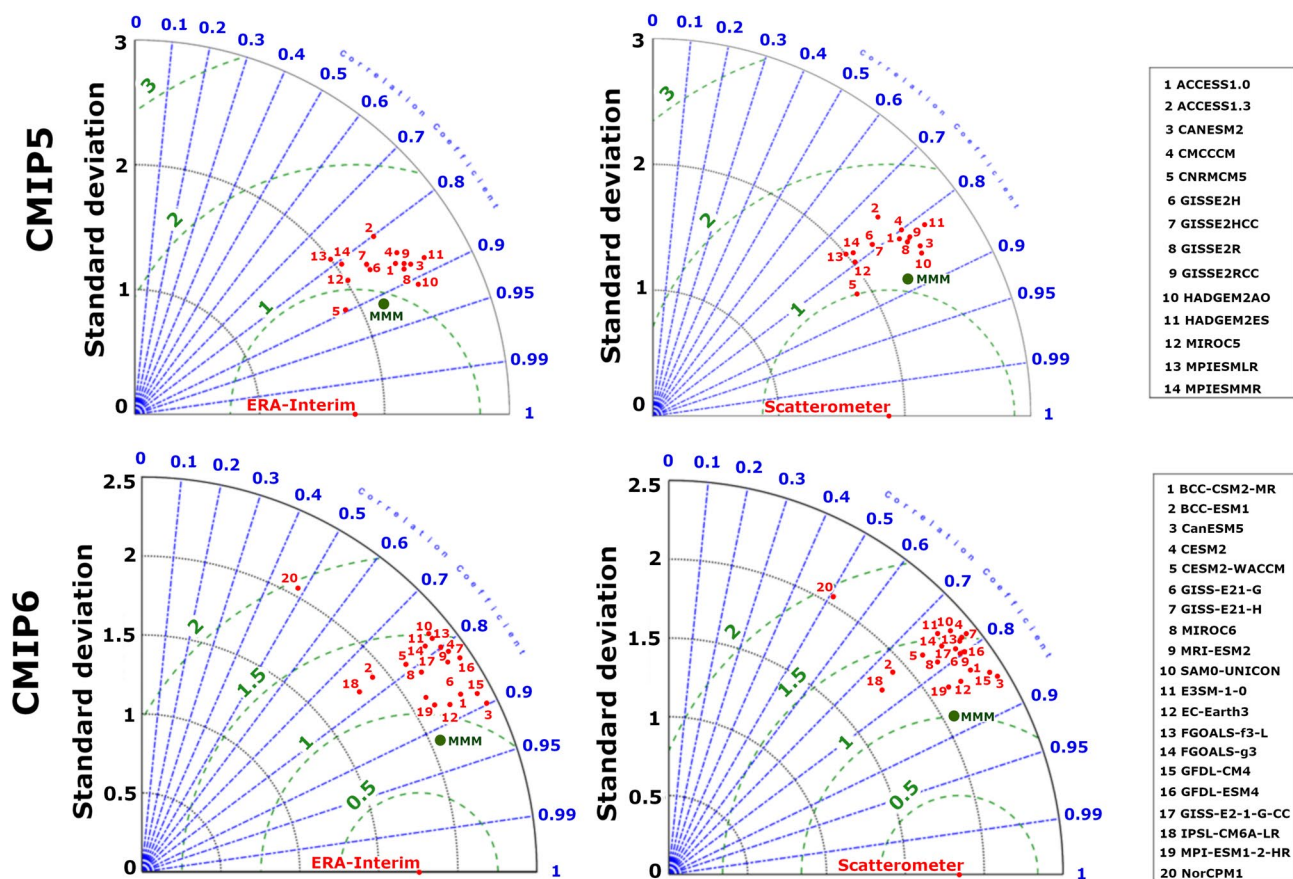


Fig. 2 Taylor diagrams of monthly mean wind speed in Bay of Bengal based on CMIP5 models (top panels) and CMIP6 models (bottom panels) along with the multi-model mean (MMM) and its comparison against ERA-interim reanalysis and scatterometer for the historical period

are chosen for spatial analysis. They are ACCESS-1.0, CanESM2, CNRM-CM5, GISS-E2R, GISS-E2RCC, and HadGEM2-ES from CMIP5 family and BCC-CSM2-MR, CanESM5, EC-Earth3, IPSL-CM6A-LR and MPI-ESM1-2-h from the CMIP6 family. The mean wind speed for 1992–2005 from ERA-interim, scatterometer, individual CMIP5 and CMIP6 models, and the Multi-Model Mean (MMM) are shown in Fig. 3.

It is seen that the wind speed distribution represented by CMIP5 and CMIP6 models vary between individual models. While CanESM2, GISS-E2R, GISS-E2RCC, and HadGEM2-ES better represents the maximum wind speed over the north-western head BoB region to an extent, they fail to represent well the other regions to match with the observations. ACCESS-1.0 was able to simulate the occurrence of higher wind speeds over other areas reasonably well with an exception for the head BoB region. Individual models under the CMIP6 family also perform differently showing varying spatial gradients in wind speed in the BoB basin. CanESM5 of CMIP6 is an upgraded version of CanESM2 in the CMIP5 family. It is noteworthy that varying spatial gradients of wind speed observed in CanESM5

model, especially for the southern BoB region and east coast of India looks superior as compared to CanESM2. General features observed in CanESM5 for the southern BoB is analogous with the reference datasets (ERA-interim and scatterometer), however there is a gross over-estimation of wind speed along the east coast of India. IPSL-CM6A-LR is the one model among CMIP6 family, which has a close resemblance with observations. The MMM estimate of wind speed from the above-mentioned individual models under CMIP5 and CMIP6 family clearly reveals that the performance of CMIP6 MMM is far superior as compared to CMIP5 MMM on comparison with observations. The CMIP5 MMM show under-estimation of wind speed in geographical regions off Andhra Pradesh coast, while the CMIP6 MMM resolved it relatively better. The efficiency of MMM is evaluated by calculating the correlation and bias error concerning the reference datasets.

It is noted from Fig. 4 that the MMM constructed from CMIP5 and CMIP6 in general correlates well with both ERA-interim and scatterometer datasets. The lower correlation identified in the shelf regions off north-western Sri Lanka, head BoB, and coastal waters off Yangon in

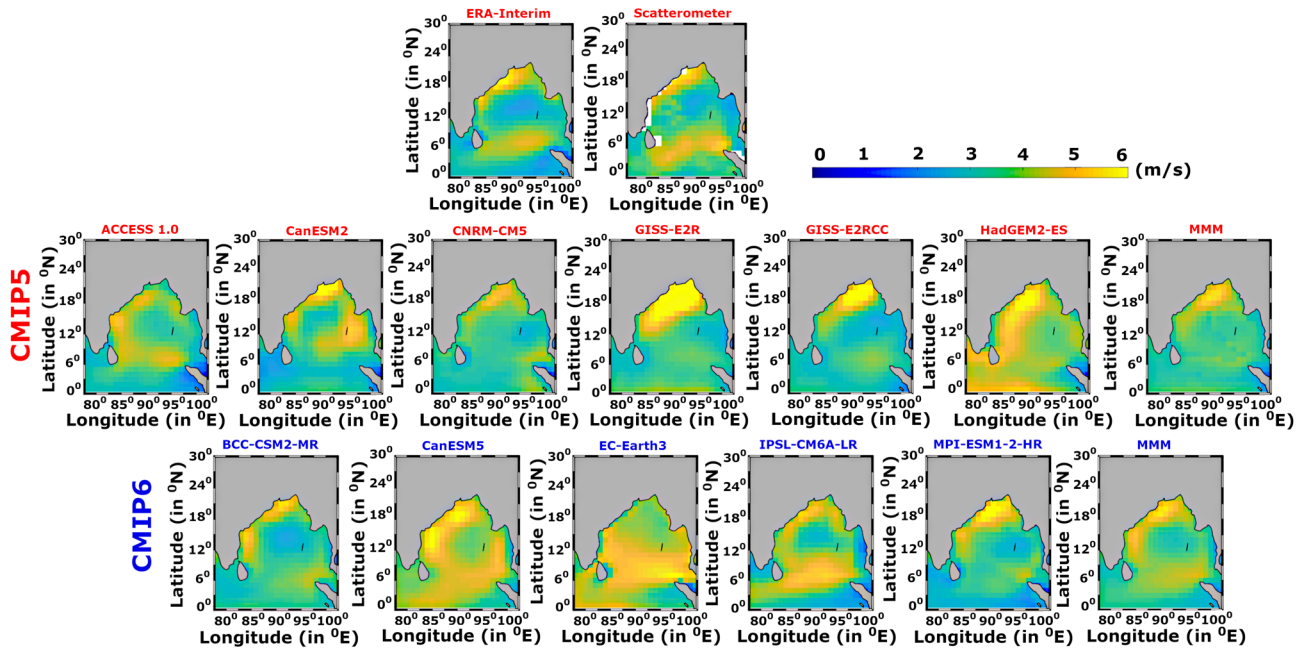


Fig. 3 Mean wind speed for the period 1992–2005 corresponding to the best performing models under CMIP5 and CMIP6 family along with reference datasets

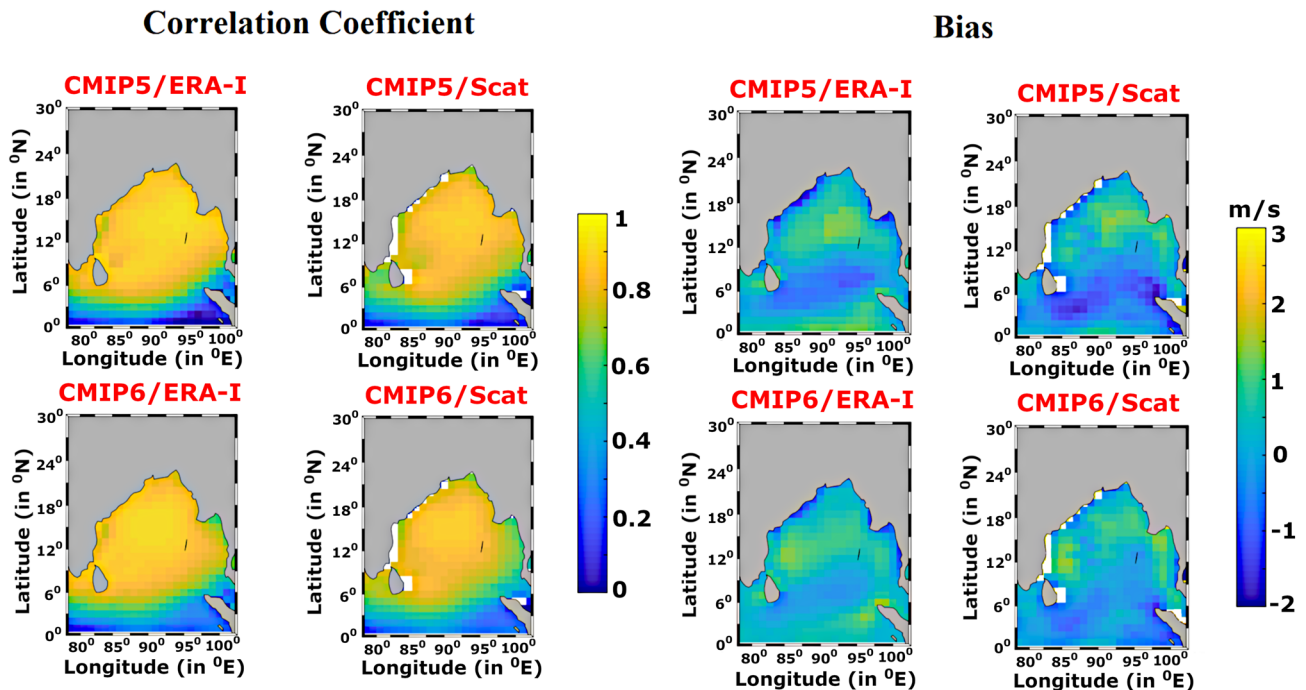


Fig. 4 Spatial distribution of correlation coefficient and bias error of multi-model mean (MMM) compared against ERA-interim and scatterometer data

Myanmar, and south-western regions off Myanmar in the Andaman Sea are due to the inherent limitations of scatterometer data in coastal regions. In the equatorial region and in the central BoB, the correlation and bias estimates of

CMIP6 MMM is relatively better than CMIP5 MMM. The overall inference in the spatial bias distribution for CMIP5 MMM and CMIP6 MMM is analogous with the spatial correlation distribution. In order to verify the effectiveness of

individual models and MMM, the study was extended to evaluate the performance of scores by comparing them with ERA-interim and scatterometer datasets.

NSE coefficients are calculated for all models under CMIP5 and CMIP6 family considered in this study. Table 6 illustrates the *NSE* of models corresponding to the historical wind speed data. Taking individual models into account, CNRM-CM5 of CMIP5 GCMs holds the highest value of 0.64 against scatterometer. Moreover, the other CMIP5 models such as MIROC5, GISS-E2H, and GISS-E2HC also performed better. The average *NSE* of all best-performing GCMs in CMIP5 family against scatterometer data is 0.33, while it is 0.42 with ERA-interim. From the 20 models of CMIP6, MPI-ESM12-HR possess a *PS* of 0.6 and in the ‘good’ category with ERA-interim and scatterometer. The reasonable models with *NSE* values between 0.4 and 0.6 are IPSL-CM6A-LR, EC-Earth3, BCC-CSM2-MR, and GISS-E21G. Furthermore, the study signifies that the MMM bears a better *NSE* value than the individual models, which are 0.62, 0.64, and 0.71 and 0.72 for CMIP5 and CMIP6 compared to the scatterometer and ERA-interim, respectively. The MMM constructed from the best performing models selected based on the Taylor skill score predicts the wind speed values reasonably well for CMIP6 than CMIP5.

Spatial correlation and bias distribution of selected CMIP6 models are shown in Figs. 5 and 6 respectively. The

correlation is less near the equatorial regions and higher over the central BoB. Models BCC-CSM2-MR, CanESM5, and MPI-ESM12-HR exhibits high correlation and less deviations from observation in terms of bias error (Fig. 6). Maximum underestimation by the models up to 2 m/s are seen along coastal areas bordering the BoB, in particular for the head BoB region. Models such as CanESM5 and EC-Earth are found to over-estimate wind speed by 2–3 m/s over the north-western areas in central BoB. From the observed trends in correlation coefficient and bias error between individual best-performing models, the MMM quantitatively enhances the performance exhibited by individual models. The *NSE* of CMIP6 MMM (Table 6) is noteworthy and higher as compared to individual models having significant implications in application-based studies. Prior studies using 33 models from CMIP5 family observed a maximum bias of 4 m/s for wind speed when compared with Altimeter data, ERA-interim, and CFSR datasets (Krishnan and Bhaskaran 2019b). Therefore, the present study clearly signifies the improved performance in CMIP6 models that eventually minimizes the biases in simulations.

Further, the assessment of models was carried out by comparing them with in situ RAMA buoy observations in BoB. Three buoys deployed over the central BoB participating in the RAMA buoy program together provide wind speed information for 7 years (2008–2014). The frequency

Table 6 Nash–Sutcliff efficiency (NSE) values estimated for CMIP5 and CMIP6 models against ERA-interim and scatterometer datasets

CMIP5 models	Nash–Sutcliff efficiency		CMIP6 Models	Nash–Sutcliff efficiency	
	GCM vs Scatterometer	GCM vs Era-I		GCM vs Scatterometer	GCM vs Era-I
ACCESS1.0	0.27	0.37	BCC-CSM2-MR	0.52	0.49
ACCESS1.3	0.19	0.25	BCC-ESM1	0.37	0.24
CANESM2	0.19	0.37	CanESM5	0.32	0.10
CMCCCM	0.31	0.36	CESM2	0.26	0.09
CNRMCM5	0.64	0.69	CESM2-WACCM	0.38	0.28
GISSE2H	0.48	0.46	GISS-E21-G	0.46	0.44
GISSE2HCC	0.46	0.46	GISS-E21-H	0.17	0.05
GISSE2R	0.36	0.42	MIROC6	0.41	0.33
GISSE2RCC	0.30	0.39	MRI-ESM2	0.33	0.17
HADGEM2AO	0.15	0.33	SAM0-UNICON	− 0.15	− 0.58
HADGEM2ES	0.31	0.39	E3SM-1-0	0.21	0.09
MIROC5	0.57	0.55	EC-Earth3	0.56	0.54
MPIESMLR	0.16	0.38	FGOALS-f3-L	− 0.15	− 0.61
MPIESMMR	0.23	0.40	FGOALS-g3	0.33	0.27
MMM	0.62	0.64	GFDL-CM4	0.24	− 0.04
			GFDL-ESM4	0.14	− 0.09
			GISS-E2-1-G-CC	0.42	0.38
			IPSL-CM6A-LR	0.54	0.61
			MPI-ESM1-2-h	0.60	0.61
			NorCPM1	− 0.17	− 0.47
			MMM	0.72	0.71

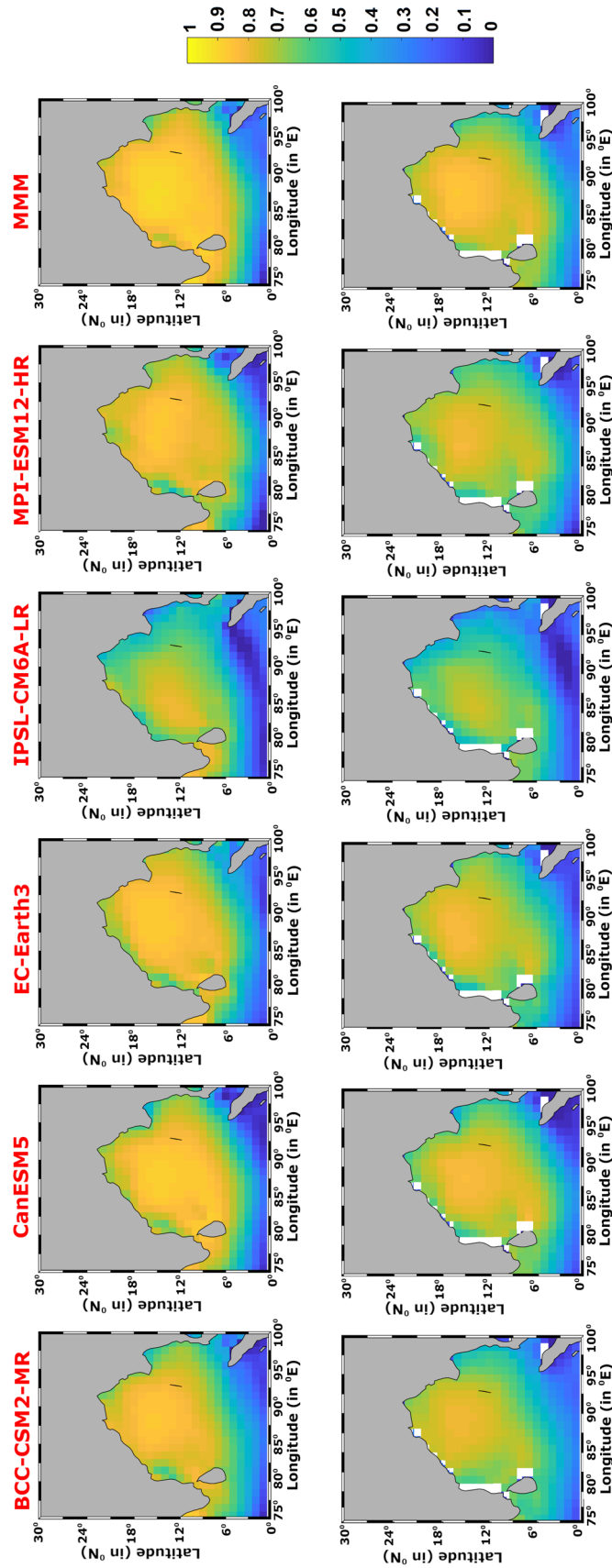


Fig. 5 Spatial distribution of correlation coefficient corresponding to the best performing models under CMIP6 family against ERA-interim (upper panel) and scatterometer data (lower panel)

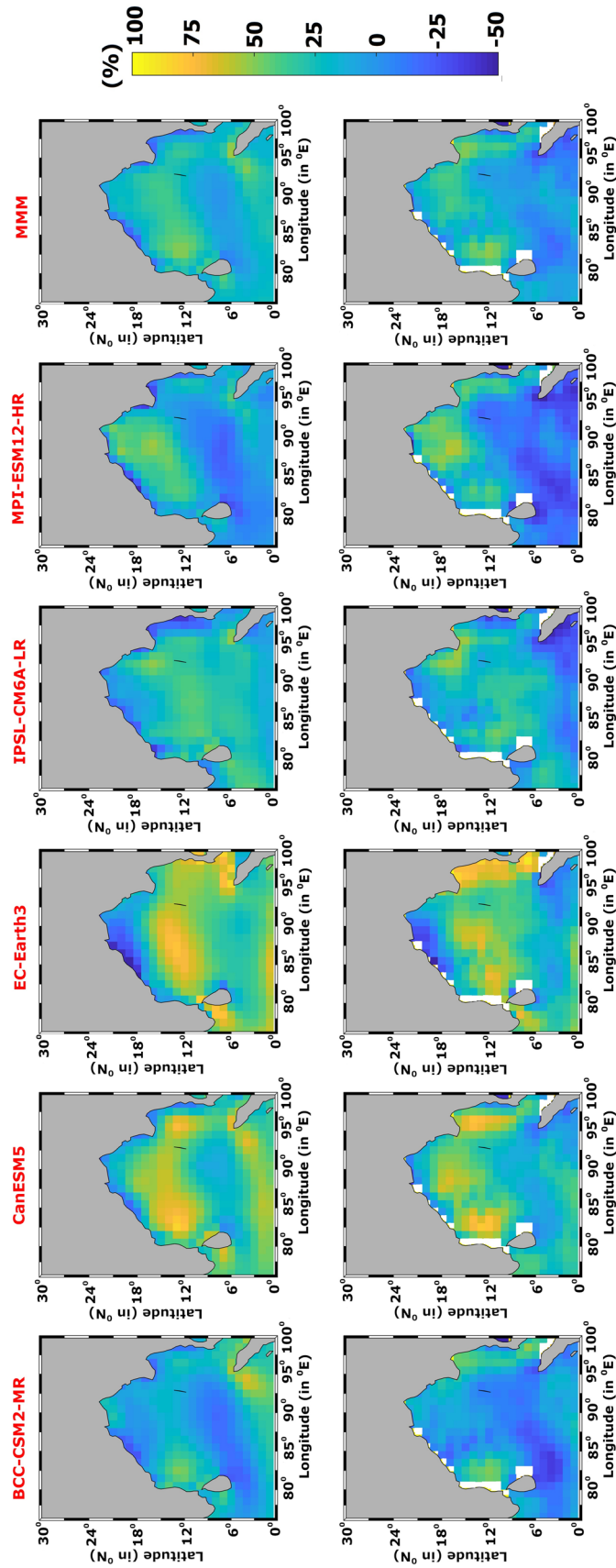


Fig. 6 Spatial distribution of bias error (in %) corresponding to the best performing models under CMIP6 family against ERA-interim (upper panel) and scatterometer data (lower panel)

of tropical cyclones is high over the BoB than in the Arabian Sea, and the central BoB is reported as an active tropical cyclogenesis generating area (Sahoo and Bhaskaran 2016). Occurrence of these extreme weather events also leads to rise in wind speed over these areas especially during the pre- and post-monsoon seasons (Shanas and Sanil Kumar 2015). A previous study by Krishnan and Bhaskaran (2019a) compared CMIP5 models against RAMA buoys and also evaluated the skill level of GCMs in simulating wind speed during cyclones in the BoB region. The study indicates that models underestimate the wind speed recorded by the buoys, primarily attributed due to coarse-resolution of GCMs in resolving the features of tropical cyclones. This study examined the performance of upcoming CMIP6 models validated against the RAMA buoys.

Figure 7 shows the time series comparison of wind speed datasets obtained from individual models of CMIP6 family, MMM based on the best performing models, and the RAMA buoy observations. As seen from this comparison, few of the individual models are either overestimating or underestimating the observations. However, the MMM established a moderate agreement with the RAMA buoy time series distribution except for a few months. Analysis reveals that maximum deviation in the GCMs are observed during the summer months of 2010, and thereafter the MMM closely follows the observations reasonably well. For the winter months with low wind speeds, the models are found to slightly overestimate the RAMA buoy observations during 2009, 2010, and 2014. The statistical measures for this comparison such as *R*, bias, *RMSE*, *NSE*, and *IA* are tabulated and shown in Table 7. The models CanESM5, GFDL-CM3, MPI-ESM12-HR, EC-EARTH3, and BCC-CSM2-MR belongs to category having the highest correlation amongst the 20 models from CMIP6 family when compared against

Table 7 Validation statistics of CMIP6 models against RAMA buoy

Models	CC	Bias (m/s)	RMSE (in m/s)	NSE	IA
BCC-CSM2-MR	0.73	0.35	1.70	0.26	0.84
BCC-ESM1	0.64	0.65	1.80	0.17	0.78
CanESM5	0.83	0.93	1.69	0.27	0.85
CESM2	0.70	0.59	1.80	0.16	0.81
CESM2-WACCM	0.52	0.23	1.97	0.00	0.73
E3SM1-0	0.72	0.63	1.73	0.23	0.82
EC-EARTH3	0.78	0.19	1.40	0.50	0.88
FGOALS-F3	0.68	1.23	2.13	-0.17	0.76
FGOALS-G3	0.66	0.29	1.74	0.22	0.80
GFDL-CM3	0.82	1.05	1.72	0.24	0.84
GFDL-ESM4	0.72	0.79	1.83	0.14	0.81
GISS-E21-G	0.72	0.13	1.63	0.32	0.84
GISS-E21G-CC	0.71	0.02	1.66	0.29	0.83
GISS-E21-H	0.70	0.23	1.68	0.27	0.83
IPSL-CM6A-LR	0.63	-0.71	1.86	0.11	0.77
MIROC6	0.71	-0.10	1.49	0.43	0.84
MPI-ESM12-HR	0.81	0.10	1.33	0.54	0.90
MRI-ESM2	0.76	0.51	1.59	0.35	0.85
NOR-CPM1	0.39	0.37	2.37	-0.44	0.63
SAM0-UNICON	0.72	1.22	2.10	-0.14	0.77
MMM	0.84	0.17	1.15	0.66	0.91

Bold values indicate the significant value

RAMA buoy data. Models such as MPI-ESM12-HR, GISS-E21G-CC, GISS-E21G, and EC-Earth has a lower bias within the range of 0.1–0.2 m/s. Study also signifies that the models with higher correlation show low *RMSE* values of 1.3–1.7 m/s with RAMA buoy observations. In addition, the MMM exhibits higher correlation and lower *RMSE* than the single models, 0.84 and 1.15 m/s, respectively. Evaluating other statistical measures for

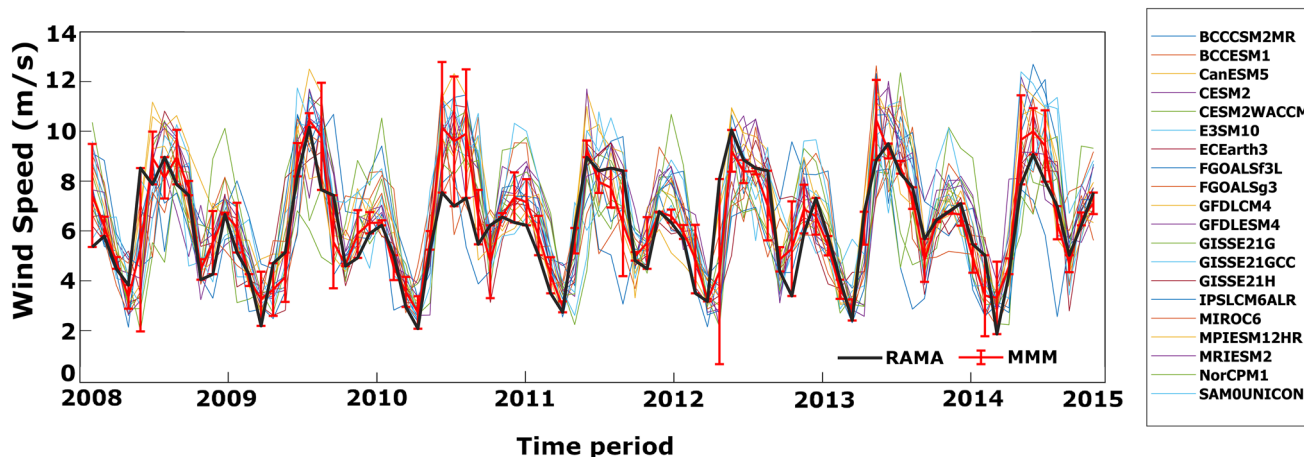


Fig. 7 Time series comparison of in situ wind speed data obtained from individual CMIP6 models (thin lines), multi-model mean MMM (thick solid red line) and the error bars show the difference of MMM from RAMA buoy observations

the goodness-of-fit such as *NSE* and *IA*, the study clearly reveals on the superior performance of MMM. From *PS*, the models EC-EARTH3, MIROC-6, and MPI-ESM12-HR have *NSE* values in a moderate range of 0.5, 0.43, and 0.54 respectively, and MMM fits into a good range with *NSE* value of 0.66. An index of agreement (*IA*) value close to 1 shows the best match for the datasets. The models, with exception for NOR-CPM1, FGOALS-F3, BCC-ESM1, IPSL-CM6A-LR, CESM2-WACCM, and SAM0-UNICON shows an *IA* value ranging between 0.8 and 1.0. While the maximum agreement obtained for models MPI-ESM12-HR, EC-EARTH3, and CanESM5 are close to 0.9, the MMM shows an *IA* value of 0.91 at the higher side. Based on the statistical estimates the study recommends that EC-EARTH3 and MPI-ESM12-HR are the two models in CMIP6 family that performed the best among the GCMs. From these several proven methods, CMIP6 models and MMM constructed from the best performing models are suitable for investigating the projected wind speed patterns over the BoB. It is clear from Table 8 that the scatterometer data for 1992–2005 had a significant higher trend with a *p* value (0.0171).

4.2 Evaluation of CMIP6 multi-model-mean projections

Projected near-surface wind speed data are extracted from the best-performing models based on the above-mentioned inter-comparison exercise under the CMIP6 family. The remarkable performance of MMM motivated to carry out the analysis on the future expected variability. The study constructed multi-model ensemble mean using the models under four SSPs, SSP1-2.6, SSP2-4.5, SSP3-7.0, and SSP5-8.5, respectively. Expected future changes for BoB under different RCP scenarios have been verified by Mohan and Bhaskaran (2019b) well in detail. Their study pointed out a substantial increase in wind speed for the head BoB and central BoB under RCP 4.5 and RCP 8.5 by the end-century. While CMIP5 discussed on the RCP scenarios with different rates of greenhouse gas emissions, CMIP6 launched a new set of SSP scenarios, which deals with the CO₂ and non-CO₂ emissions in different ways. The futuristic variations of RCP scenarios and SSP pathways are clearly depicted in Fig. 8. The SSP scenarios begin from 2015, where RCP scenarios were from 2006 onwards. The low-end scenario SSP1-2.6 has a more gradual decline than RCP 2.6 because the emissions during 2006–2014 were higher than expected

Table 8 Mann Kendall significance test with Theil–Sen estimates

Datasets	CMIP5		Datasets	CMIP6	
	<i>p</i> value (two tailed)	Sen slope		<i>p</i> value (two tailed)	Sen slope
Scatterometer	0.0171	0.0069	Scatterometer	0.0654	0.0027
ERA-interim	0.7649	0.0009	ERA-interim	0.5850	0.0008
ACCESS1.0	0.9628	0.0002	BCC-CSM2-M	0.7168	0.0006
ACCESS1.3	0.7628	0.0010	BCC-ESM1	0.5461	0.0009
CANESM2	0.6459	0.0019	CanESM5	0.5276	0.0010
CMCCM	0.8574	0.0006	CESM2	0.9267	0.0002
CNRMCM5	0.7859	0.0009	CESM2-WACCM	0.9050	– 0.0002
GISSE2H	0.9322	0.0003	GISS-E21-G	0.5783	0.0008
GISSE2HCC	0.9847	0.0000	GISS-E21-H	0.6362	– 0.0007
GISSE2R	0.6888	0.0014	MIROC6	0.8118	0.0004
GISSE2RCC	0.6647	0.0015	MRI-ESM2	0.8555	0.0003
HADGEM2AO	0.8822	– 0.0004	SAM0-UNICON	0.8087	0.0005
HADGEM2ES	0.9072	0.0004	E3SM-1-0	0.5422	0.0011
MIROC5	0.7183	– 0.0012	EC-Earth3	0.7046	0.0006
MPIESMLR	0.6677	0.0014	FGOALS-f3-L	0.9184	– 0.0002
MPIESMMR	0.6717	0.0015	FGOALS-g3	0.9932	0.0000
MMM	0.6888	0.0009	GFDL-CM4	0.9019	– 0.0002
			GFDL-ESM4	0.6844	– 0.0007
			GISS-E2-1-G-CC	0.9106	0.0002
			IPSL-CM6A-LR	0.7153	– 0.0005
			MPI-ESM1-2-h	0.8643	0.0003
			NorCPM1	0.5149	0.0011
			MMM	0.6738	0.0004

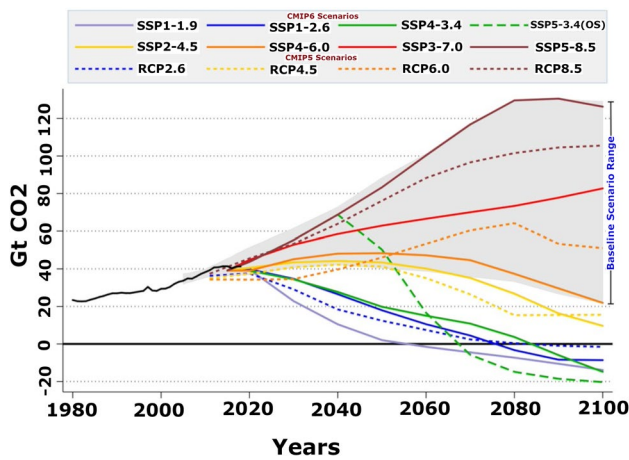


Fig. 8 Future representative concentration pathway (RCP) CO₂ emission scenarios featured in CMIP5 and their CMIP6 counterparts. (historical CO₂ emissions in black). (Source URL: <https://www.carbonbrief.org/cmip6-the-next-generation-of-climate-models-explained>)

by RCP-2.6. In the case of SSP2-4.5, the non-CO₂ plays a role and causing a higher starting point than RCP 4.5. The transformation of emissions attaining its peak and declining trend for RCP 6.0 and SSP3-7.0 follows the period 2080 and

2050, respectively. The scenario representing the worst-case SSP5-8.5 is much higher than RCP 8.5, with correspondingly more massive cuts in non-CO₂ emissions.

There are no studies attempted on projected changes in wind speed over the global ocean basins utilizing the new GCMs developed under the CMIP6 project. Changing climate scenario caused by global warming warrants special attention to specifically study and understand their impact on the regional patterns of ocean and atmospheric variables. Dealing with the wind speed projections under four SSP scenarios, the linear trends in 25 years of data has been investigated. The historical data for 1990–2014 is used as a reference, and the near future (2026–2050), mid-century (2051–2075), and end-century (2076–2100) are selected to distinguish the changes. The projected wind speed data are divided into three durations in order to understand the expected future under different emission scenarios and to quantify the variability from the past data. The observed linear trends in the MMM projected wind speeds are shown in Fig. 9. As seen from this figure, the spatial distribution concerning the rate of change in wind speed per year over BoB show distinct patterns under each SSP scenario. Based on the historical trend values, it is evident that wind speed has increased over the central BoB and neighbouring

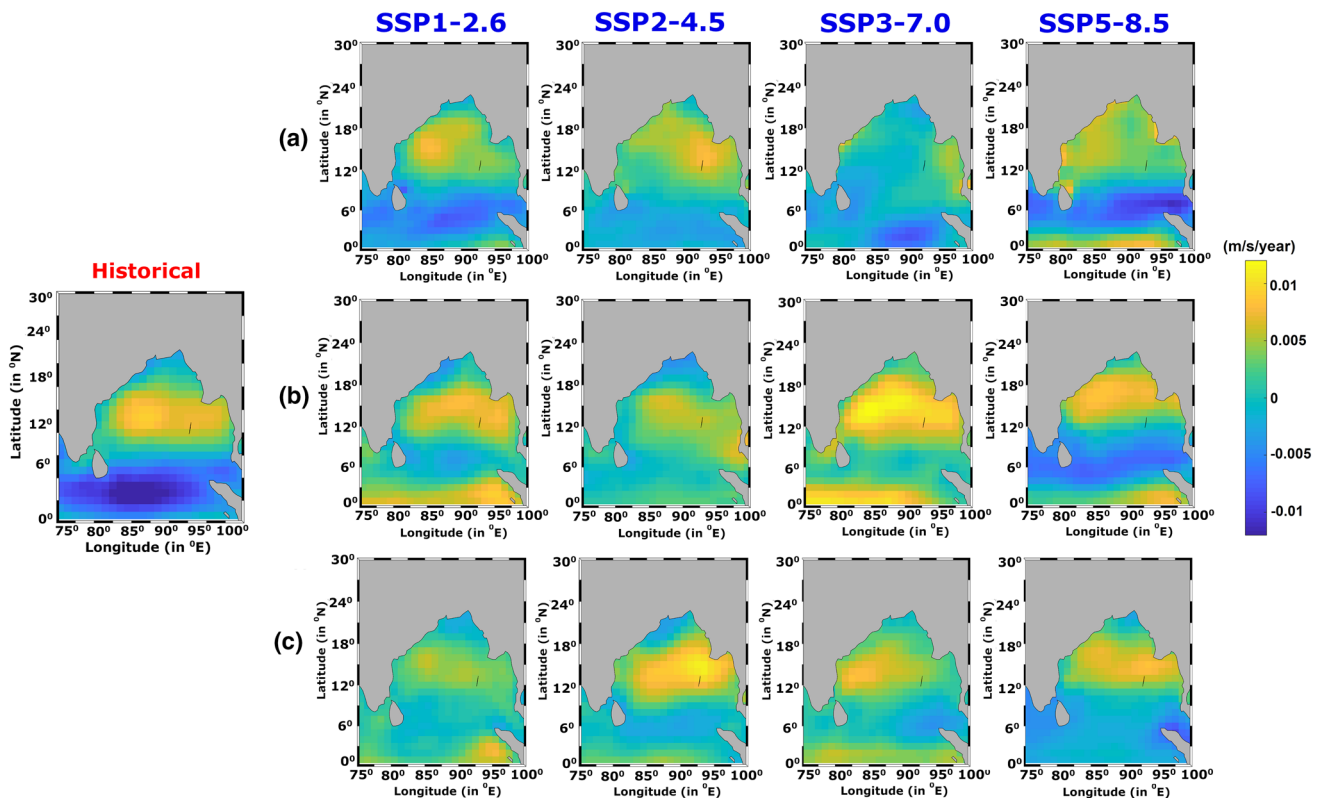


Fig. 9 Trends in the multi-model mean (MMM) projected wind speed based on historical run (1990–2014), **a** near future (2026–2050), **b** mid-century (2051–2076), and **c** end-century (2076–2100)

regions, while it has reduced near the equatorial regions. Rising SST imparted by global warming resulted in various disturbances in the atmospheric circulations. The variations in wind speed are closely related to the changes in sea surface temperature (SST) and sea level pressure distributions. Wallace et al. (1989) reported that atmospheric boundary layer plays a vital role in the variation of wind speed with SST gradients. They suggest that warm waters reduce wind shear near sea-surface and thereby wind speed increases. Another model by Lindzen and Nigam (1987) related the SST by hydrostatic pressure gradients induced in the marine atmospheric boundary layer. Chelton et al. (2004) identified that the net effects of SST on marine boundary layer would increase the wind speed regime over warm waters. SST analysis during 1985–1998 using in-situ data along the coastal waters of head BoB region showed an increasing trend (Khan et al. 2000). A significant positive trend in SST was reported (Jadhav and Munot 2009) for BoB after 1960. Furthermore, a negative correlation is established between SST and wind speed in most of the studies and evident for BoB (Sinha et al. 2020). Increased SST trend reduces the sea level pressure and suppress the atmospheric lower layer circulation, which leads to weakening of the wind speed (Mohan and Bhaskaran 2019b). In the near future, the low-end scenario (SSP1-2.6) showed a rise in wind speed over north-western regions of BoB, which is seen extending zonally southward leading to a rise for regions near the equator during the mid-century and reduces by the end-century. The case SSP2-4.5, where non-CO₂ emissions declines, illustrate a weak positive trend in wind speed, which peaks during end-century over the north-eastern regions (off Myanmar) in the study area. In the middle of the road scenario, SSP3-7.0 showed maximum increasing trends during the mid-century, and a medium stabilizing scenario by the end-century. SSP5-8.5 layout a warm world with business as a usual condition among possible no-policy outcomes demarcates rise in wind speed along the east coast of India in near-future scenario and extends to latitude range of 12° N–20° N and declining trend during the mid- and end-century respectively. End-century results for the worst scenario follows a similar trend of mid-century for those areas with the rise and declining trend changes to neutral for other areas. In general, the study signifies that equatorial regions will be experiencing higher wind speeds as compared to the present. The variability in wind speed projected under various scenarios of emissions has been quantified by calculating the percentage change in the future with reference to the historical data.

Figure 10 represents the projected changes in wind speed using the MMM dataset. The percentage change in MMM wind speed distribution in the near-future, mid-century, and end-century periods are evaluated, keeping historical simulations for 1990–2014 as the reference. The maximum rise of 25% (0.5–1 m/s) in wind speed is observed for the

SSP3-7.0 scenario over the central and southern BoB for the near future, and this trend was found to decrease in the later decades. A decline in wind speed by 0.2–0.8 m/s has been projected over the head BoB and neighbouring regions for the near future under the SSP1-2.6 scenario. An increase of 5–20% in wind speed is noticed for the east coast of India and head BoB regions under the SSP2-4.5 scenario. The high-end scenario, SSP5-8.5 shows a slight increase in wind speed over BoB by 0.2–0.6 m/s for the near future, whereas those coverage that experience higher wind speeds over northern BoB continue to a decline by 0.8 m/s for the mid-century. Thereafter, an opposite trend is noted in the spatial distribution of wind speed over the BoB region. Geographical areas over the head BoB experiences a rise and an overall decrease is noticed for the central and southern BoB regions. A recent study indicates decrease in future wind speed for regions north of the equator projected using a super high-resolution MRI-AGCM3.2S model (Kamranzad and Mori 2019). However, the climate models primarily discuss the warming world, and the resulting projections helps to frame development policies, the rise or fall in temperature causes complementary variations in other parameters such as wind speed. The decline in end-century wind speed projections (Fig. 10c) evidenced by the worst scenario over major areas in BoB can possibly be the outcome resulting from rise in SST. Annual variations obtained from monthly datasets of wind speed from GCMs has a tendency to average out the seasonal changes and their effects on the parameter. Therefore, the present study also deals with the seasonal patterns of futuristic wind speed projected over the BoB.

The monsoon wind system plays a pivotal role in determining the climate system over the NIO basin influencing the semi-marginal seas AS and BoB. During the winter months of December–January–February (DJF), a high-pressure system over the north BoB produces the north-east monsoon. The south-west monsoon season prevails in June–July–August (JJA) months resulting in subsequent airflow from the ocean. The characteristic wind speed distributions for the two seasons are represented in Figs. 11 and 12. The warm SST that prevails during the summer monsoon months over the BoB and huge influx of freshwater from riverine sources create an interaction between ocean and atmosphere (Goswami et al. 2016). During the onset of monsoon, the south-westerly winds intensify over the BoB (Krishnamurthy and Kirtman 2003) reaching up to 12 m/s for the northern BoB (Bhat et al. 2001). The projected changes in wind speed for JJA show a slight increase/decrease by 5–15% for the northern BoB and southern BoB regions, respectively, under all scenarios for the near future (Fig. 11a). A recent study by Patra and Bhaskaran (2016) found variations in wind speed for BoB based on analysis of satellite altimeter data during the monsoon season (June–September). The variations noticed was about 15%

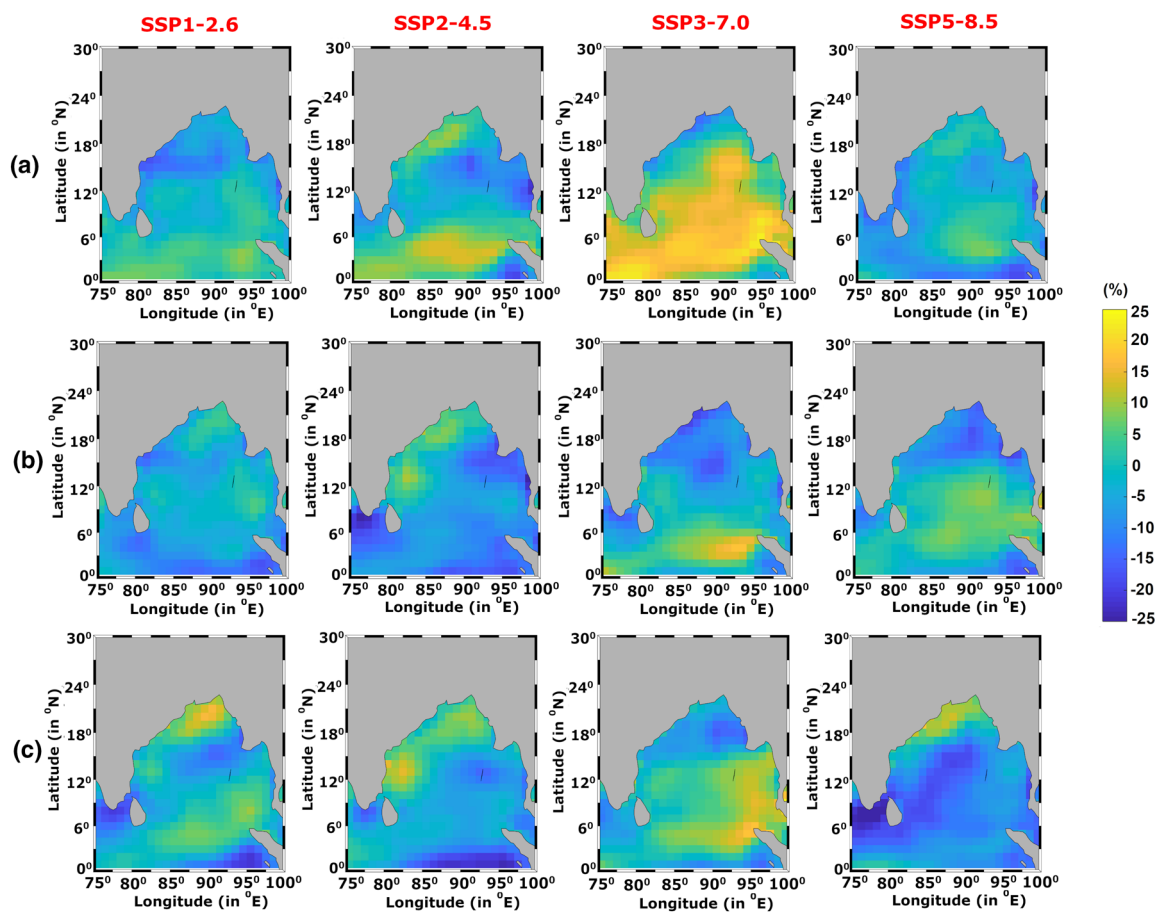


Fig. 10 Percentage changes in the multi-model mean (MMM) projected wind speed for **a** near future (2026–2050), **b** mid-century (2051–2076), and **c** end-century (2076–2100) relative to the historical period (1990–2014)

during the period 1992–2012. The estimated change of 15% as seen in the near-future projections are consistent with the change noticed from the observations. Though the spatial distribution looks similar under all the forcing scenarios, the relative strength of wind speed is found increasing for the mid-century and end-century MMM projections. The mid- and end-century projected changes under SSP3-7.0 and SSP5-8.5 scenarios demarcate a decrease in wind speed up to 15% for the southern BoB, except for equatorial regions. Further, the seasonal distribution for summer months show a significant rise in projected wind speed over the head BoB, which is expected to strengthen the magnitude from low-end to high-end scenarios.

During the winter months of DJF, the changes in wind speed follow an opposite pattern unlike JJA months. Regions that experience a rise in future wind speed are located over the central BoB, that is expected to rise a maximum of 30% from the historical. Patra and Bhaskaran (2016) also pointed out that the winter months (DJF) showed a 20% increase in wind speed based on analysis using the altimeter data during 1990–2012. Similar to the

JJA distribution, near-future decades of DJF are also not susceptible to large differences from past under any of the climate change scenarios. However, the changes are found to intensity from 2050 onwards, and that is common in all emission scenarios. The trend looks different for the head BoB region that show a negative projected change in wind speed by 20% unlike the other regions over the BoB. This can be attributed due to significant warming over the head BoB region observed during the past decades (Patra et al. 2018). Mid-century and end-century projections under SSP3-7.0 and SSP5-8.5 are expected to increase over regions in the head BoB, the southern mainland of India, off Sri Lanka, and off Myanmar. Southern BoB and equatorial regions will experience a positive change of 5–15% rise in wind speed. The cooling phase of BoB during DJF (Srivastava et al. 2016) after the warmer months could be a possible reason for the intensification of wind speed over the central BoB. Therefore, the variability and distribution of near-surface wind speed over BoB, making use of historical and projected datasets has been discussed under different emission scenarios of climate change.

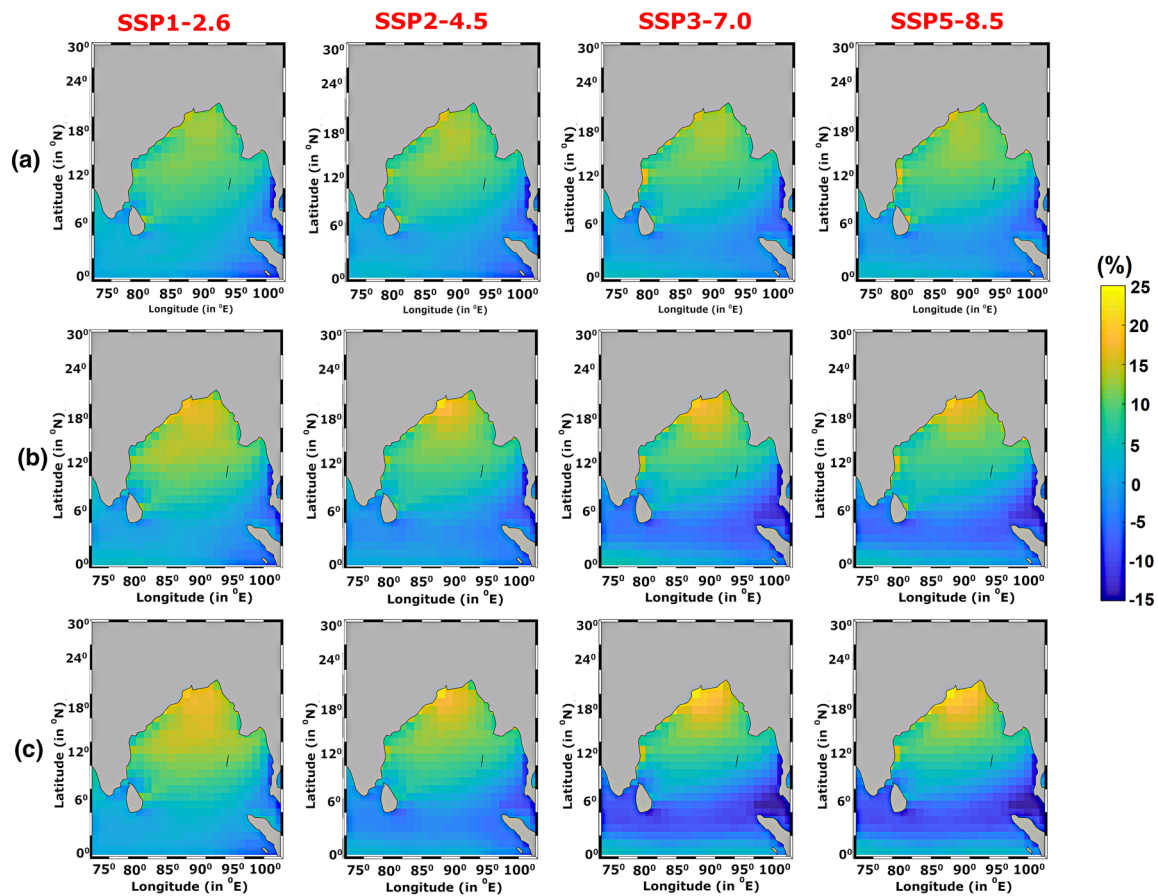


Fig. 11 Percentage changes in the Multi-Model Mean (MMM) surface wind speed over the Bay of Bengal during summer (JJA) for **a** near future (2026–2050), **b** mid-century (2051–2076), and **c** end century (2076–2100) relative to the historical period (1990–2014)

5 Conclusions

This study verifies the impact of climate change on wind speed characteristics over the BoB, making use of GCMs developed under the CMIP project. The historical wind speed datasets simulated by CMIP5 and CMIP6 models are compared against scatterometer, ERA-interim reanalysis, and in-situ RAMA buoys. Improved capability of CMIP6 than CMIP5 models in simulating wind speed has been observed based on various inter-comparison exercises and statistical estimates. The models BCC-CSM2-MR, CanESM5, EC-EARTH3, IPSL-CM6A-LR, and MPI-ESM12-HR are identified as the best-performing models under CMIP6 family in simulating wind speed in the BoB. The MMM constructed from best performing CMIP6 models were selected for further analysis investigating the projected changes in wind speed. Future changes in wind speed over the BoB domain are evaluated for different scenarios such as near-future (2026–2050), mid-century (2051–2075), and end-century (2076–2100) relative to the historical period of 1990–2014 under four different emission scenarios of CMIP6. The projected MMM wind speed

for the near-future, mid-century, and end-century showed a rising trend for northern BoB regions under all forcing scenarios and along with a decline over the southern BoB under SSP5-8.5. The spatial distributions of wind speed hold an inverse relationship for summer (JJA) and winter (DJF) seasons. The southwest monsoon winds over the head BoB are projected to change positively up to 15% for the near-century and it intensifies to 25% during the end-century from the historical period under SSP3-7.0 and SSP5-8.5 respectively. In contrast, the winter season experiences a decreasing intensity over the head BoB and increase over the central BoB, which is apparent in all the forcing scenarios maintaining a rise in magnitude from SSP1-2.6 to SSP5-8.5. Irrespective of seasons, a net increase of 0.6–0.8 m/s has been observed for the east coast of India under SSP2-4.5 for the mid and end of the twenty-first century. A maximum rise of 25% (0.5–1 m/s) in wind speed is observed for the SSP3-7.0 scenario over the BoB for the near-future. Furthermore, a decline of 0.2–0.8 m/s in wind speed has been noticed in the central and southern BoB under the extreme scenario of SSP5-8.5. The simulated outputs in the form of future projections generated by these climate models are highly

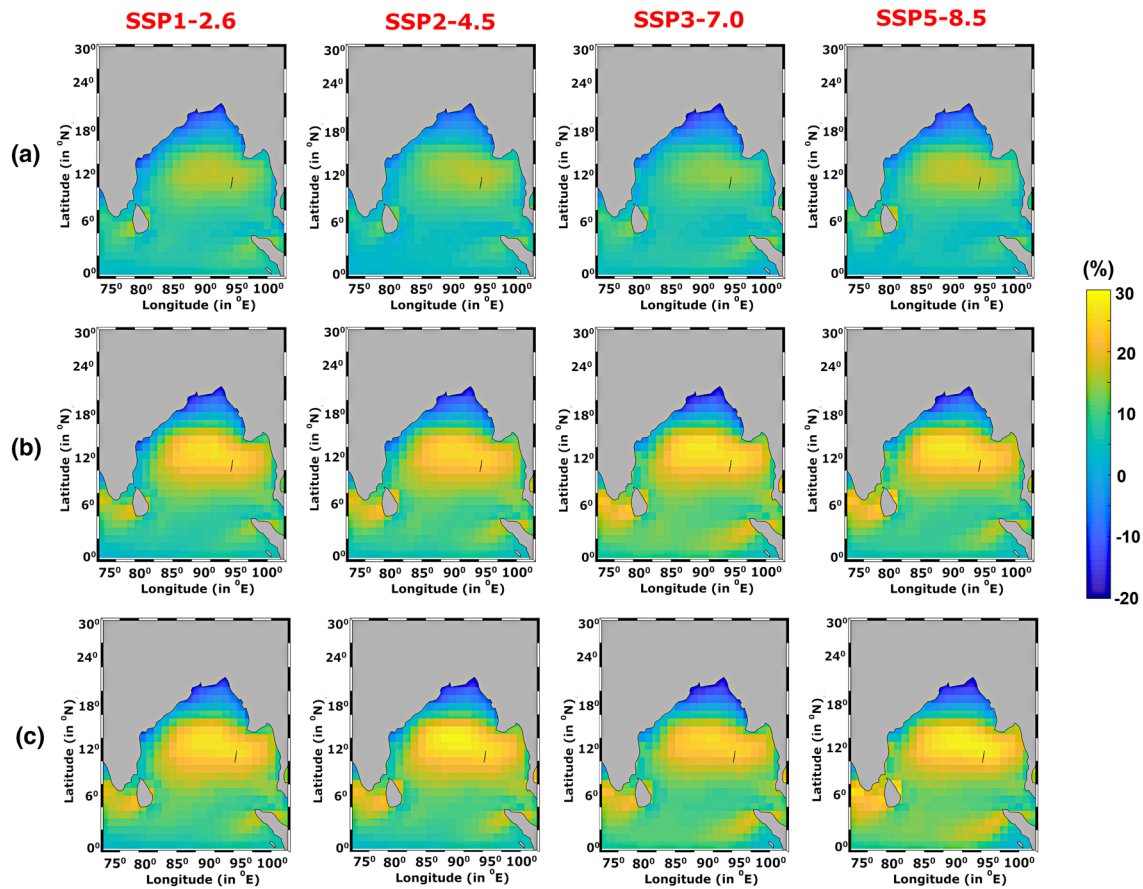


Fig. 12 Percentage changes in the multi-model mean (MMM) surface wind speed over the Bay of Bengal during winter (DJF) for **a** near future (2026–2050), **b** mid-century (2051–2076), and **c** end century (2076–2100) relative to the historical period (1990–2014)

dependent on the underlying physics such as parameterization of convection schemes, the inclusion of carbon cycle dynamics, and model resolutions in representing mesoscale and sub-mesoscale topographies. The better skill demonstrated by CMIP6 models than CMIP5 models noted from this study must be attributed to advancements made in model physics and parameterization of physical processes. Moreover, the amount of bias sustained in the current models are needed to be accounted for, and a detailed study utilizing many more models under CMIP6 family will be separately done in future work.

Acknowledgements The authors sincerely thank the Department of Science and Technology (DST), Government of India, for the financial support. This study was conducted under the Centre of Excellence (CoE) in Climate Change studies established at IIT Kharagpur funded by DST, Government of India. The study forms a part of the ongoing project 'Wind-Waves and Extreme Water Level Climate Projections for the East Coast of India'. The authors also acknowledge the World Climate Research Program's Working Group on Coupled Modelling, for providing CMIP5 and CMIP6 multi-model data, Asia-Pacific Data Research Center for the scatterometer data from ERS-1/2, QuikSCAT, and ASCAT satellite missions, the European Centre for Medium-Range Weather Forecasts for the ERA-interim data and Pacific Marine

Environmental Laboratory under National Oceanic and Atmospheric Administration (NOAA) for the RAMA buoy observations.

References

- Abram NJ, Wright NM, Ellis B, Dixon BC, Wurtzel JB, England MH, Ummenhofer CC, Philibosian B, Cahyarini SY, Yu TL, Shen CC (2020) Coupling of Indo-Pacific climate variability over the last millennium. *Nature* 579(7799):385–392
- Bentamy A, Denis CF (2012) Gridded surface wind fields from Metop/ASCAT measurements. *Int J Remote Sen.* <https://doi.org/10.1080/01431161.2011.600348>
- Bentamy A, Croize-Fillon D, Perigaud C (2008) Characterization of ASCAT measurements based on Buoy and QuikSCAT wind vector observations. *Ocean Sci* 4(4):265–274
- Bhaskaran PK (2019) Challenges and future directions in ocean wave modeling: a review. *J Extreme Events.* <https://doi.org/10.1142/S2345737619500040>
- Bhaskaran PK, Gupta N, Dash MK (2014) Wind-wave climate projections for the Indian Ocean from Satellite observations. *J Mar Sci Res Dev* S11:005. <https://doi.org/10.4172/2155-9910.S11-005>
- Bhat GS, Gadgil S, Hareesh Kumar PV, Kalsi SR, Madhusoodanan P, Murty VSN, Prasada Rao CVK, Ramesh Babu V, Rao LVG, Rao RR, Ravichandran M, Reddy KG, Sanjeeva Rao P, Sengupta D, Sikka DR, Swain J, Vinayachandran PN (2001) BOBMEX:

- the Bay of Bengal monsoon experiment. *Bull Am Meteorol Soc* 82(10):2217–2243
- Birsan MV, Lenuta M, Alexandru D (2013) Seasonal changes in wind speed in Romania. *Rom Rep Phys* 65(4):1479–1484
- Brands S, Herrera S, Fernández J, Gutiérrez JM (2013) How well do CMIP5 earth system models simulate present climate conditions in Europe and Africa? *Clim Dyn* 41(3–4):803–817
- Brower MC, Barton MS, Lledó L, Dubois J, (2013) A study of wind speed variability using global reanalysis data. AWS Truepower. <https://aws-dewi.ul.com/assets/A-Study-of-Wind-Speed-Variability-Using-Global-Reanalysis-Data2.pdf>. Accessed 14 Jan 2020
- Carvalho D, Rocha A, Gómez-Gesteira M, Silva Santos C (2014a) Comparison of reanalyzed, analyzed, satellite-retrieved and NWP modelled winds with Buoy data along the Iberian Peninsula Coast. *Remote Sens Environ* 152:480–492
- Carvalho D, Rocha A, Gómez-Gesteira M, Silva Santos C (2014b) Offshore wind energy resource simulation forced by different reanalyses: comparison with observed data in the Iberian Peninsula. *Appl Energy* 134:57–64. <https://doi.org/10.1016/j.apenergy.2014.08.018>
- Carvalho D, Rocha A, Gómez-Gesteira M, Santos CS (2017) Potential impacts of climate change on European wind energy resource under the CMIP5 future climate projections. *Renew Energy* 101:29–40
- Celik DF, Cengiz E (2014) Wind speed trends over Turkey from 1975 to 2006. *Int J Climatol* 34(6):1913–1927
- Chelton DB, Schlax MG, Freilich MH, Milliff RF (2004) Satellite measurements reveal persistent small-scale features in ocean winds. *Science* 303(5660):978–983
- Chu PC, Qi Y, Chen Y, Shi P, Mao Q (2004) South China sea wind-wave characteristics. Part 1: validation of wavematch-III using TOPEX/poseidon data. *J Atmos Ocean Technol* 21(11):1718–1733. <https://doi.org/10.1175/JTECH1661.1>
- Crawford CG, Slack JR, Hirsch RM (1983) Nonparametric tests for trend in water quality data using the statistical analysis system. Open Report no. 83-550, US Geological Survey, USA
- Dee DP, Uppala SM, Simmons AJ, Berrisford P, Poli P, Kobayashi S, Andrae U, Balmaseda MA, Balsamo G, Bauer P, Bechtold P, Beljaars ACM, van de Berg L, Bidlot J, Bormann N, Delsol C, Dragani R, Fuentes M, Geer AJ, Haimberger L, Healy SB, Hersbach H, Holm EV, Isaksen L, Kallberg P, Kohler M, Matricardi M, McNally AP, Monge-Sanz BM, Morcrette J-J, Park B-K, Peubey C, de Rosnay P, Tavolato C, Thepaut J-N, Vitart F (2011) The ERA-interim reanalysis: configuration and performance of the data assimilation system. *Q J R Meteorol Soc* 137(656):553–597
- Dong L, Zhou T, Wu B (2014) Indian Ocean warming during 1958–2004 simulated by a climate system model and its mechanism. *Clim Dyn* 42:203–217. <https://doi.org/10.1007/s00382-013-1722-z>
- Ebuchi N, Graber HC, Caruso MJ (2002) Evaluation of wind vectors observed by QuikSCAT/SeaWinds using Ocean Buoy Data. *J Atmos Ocean Technol*. [https://doi.org/10.1175/1520-0426\(2002\)019<2049:EOWVOB>2.0.CO;2](https://doi.org/10.1175/1520-0426(2002)019<2049:EOWVOB>2.0.CO;2)
- Eyring V, Bony S, Meehl GA, Senior CA, Stevens B, Stouffer RJ, Taylor KE (2016) Overview of the Coupled Model Intercomparison Project Phase 6 (CMIP6) experimental design and organization. *Geosci Model Dev* 9(5):1937–1958
- Figa-Saldaña J, Wilson JJW, Attema E, Gelsthorpe R, Drinkwater MR, Stoffelen A (2002) The advanced scatterometer (Ascat) on the meteorological operational (MetOp) platform: a follow on for European Wind Scatterometers. *Can J Remote Sens*. <https://doi.org/10.5589/m02-035>
- Ghorbani MA, Khatibi R, FazeliFard MH, Naghipour L, Makarynskyy O (2016) Short-term wind speed predictions with machine learning techniques. *Meteorol Atmos Phys* 128(1):57–72
- Gidden MJ, Riahi K, Smith SJ, Fujimori S, Luderer G, Kriegler E, van Vuuren DP, van den Berg M, Feng L, Klein D, Calcin K, Doelman JC, Frank S, Fircko O, Harmsen M, Hasegawa T, Havlik P, Hilaire J, Hoesly R, Horing J, Popp A, Stehfest E, Takahashi K (2019) Global emissions pathways under different socioeconomic scenarios for use in CMIP6: a dataset of harmonized emissions trajectories through the end of the century. *Geosci Model Dev* 12(4):1443–1475
- Gocic M, Trajkovic S (2013) Analysis of changes in meteorological variables using Mann–Kendall and Sen’s slope estimator statistical tests in Serbia. *Glob Planet Change* 100:172–182. <https://doi.org/10.1016/j.gloplacha.2012.10.014>
- Goswami BN, Rao AS, Sengupta D, Chakravorty S (2016) Monsoons to mixing in the Bay of Bengal: multiscale air–sea interactions and monsoon predictability. *Oceanography* 29(2):18–27
- Gupta N, Bhaskaran PK (2016) Inter-dependency of wave parameters and directional analysis of ocean wind-wave climate for the Indian Ocean. *Int J Climatol* 37:3036–3043. <https://doi.org/10.1002/joc.4898>
- Gupta N, Bhaskaran PK, Dash MK (2015) Recent trends in wind-wave climate for the Indian Ocean. *Curr Sci* 108(12):2191–2201
- Gupta N, Bhaskaran PK, Dash MK (2017) Dipole behavior in maximum significant wave height over the Southern Indian Ocean. *Int J Climatol* 37:4925–4937. <https://doi.org/10.1002/joc.5133>
- Hasager CB, Dellwik E, Nielsen M, Furevik BR (2004) Validation of ERS-2 SAR offshore wind-speed maps in the North Sea. *Int J Remote Sens* 25(19):3817–3841
- Helsel DR, Hirsch RM (1992) Statistical methods. *Water Resour*. <https://doi.org/10.3133/twri04A3>
- IPCC (2013) Summary for Policymakers. In: Stocker TF, Qin D, Plattner G-K, Tignor M, Allen SK, Boschung J, Nauels A, Xia Y, Bex V, Midgley PM (eds) *Climate change. The physical science basis. Contributions of Working Group I to the Fifth Assessment Report of the Intergovernmental Panel on Climate Change*. Cambridge University Press, Cambridge
- Jadhav SK, Munot AA (2009) Warming SST of Bay of Bengal and decrease in formation of cyclonic disturbances over the Indian Region during southwest monsoon season. *Theor Appl Climatol* 96(3–4):327–336
- Kamranzad B, Mori N (2019) Future wind and wave climate projections in the Indian Ocean based on a super-high-resolution MRI-AGCM3.2S model projection. *Clim Dyn* 53(3–4):2391–2410. <https://doi.org/10.1007/s00382-019-04861-7>
- Kendall MG (1975) Rank correlation methods, 4th edn. Charles Griffin, London
- Khan TMA, Singh OP, Rahman MS (2000) Recent sea level and sea surface temperature trends along the Bangladesh Coast in relation to the frequency of intense cyclones. *Mar Geod* 23(2):103–116
- Klein SA, Soden BJ, Lau N-C (1999) Remote sea surface temperature variations during ENSO: evidence for a tropical atmospheric bridge. *J Clim* 12:917–932
- Krishnamurthy V, Kirtman BP (2003) Variability of the Indian Ocean: relation to monsoon and ENSO. *Q J R Meteorol Soc* 129(590 Part A):1623–1646
- Krishnan A, Bhaskaran PK (2019a) Performance of CMIP5 wind speed from global climate models for the Bay of Bengal region. *Int J Climatol*. <https://doi.org/10.1002/joc.6404>
- Krishnan A, Bhaskaran PK (2019b) CMIP5 wind speed comparison between satellite altimeter and reanalysis products for the Bay of Bengal. *Environ Monit Assess*. <https://doi.org/10.1007/s10661-019-7729-0>
- Kulkarni S, Huang HP (2014) Changes in surface wind speed over North America from CMIP5 model projections and implications for wind energy. *Ad Meteorol*. <https://doi.org/10.1155/2014/292768>

- Kumar P, Min SK, Weller E, Lee H, Wang XL (2016) Influence of climate variability on extreme ocean surface wave heights assessed from ERA-interim and ERA-20C. *J Clim* 29(11):4031–4046. <https://doi.org/10.1175/JCLI-D-15-0580.1>
- Kumar P, Kaur S, Weller E, Min SK (2019) Influence of natural climate variability on the extreme Ocean surface wave heights over the Indian Ocean. *J Geophys Res Oceans* 124(8):6176–6199
- Lee T, Waliser DE, Li J-LF, Landerer FW, Gierach MM (2013) Evaluation of CMIP3 and CMIP5 wind stress climatology using satellite measurements and atmospheric reanalysis products. *J Clim* 26(16):5810–5826
- Lehner S, Schulz-Stellenfleth J, Schattler B, Breit H, Horstmann J (2000) Wind and wave measurements using complex ERS-2 SAR wave mode data. *IEEE Trans Geosci Remote Sens* 38(5):2246–2257
- Lin F, Chen X, Yao H (2017) Evaluating the use of Nash–Sutcliffe efficiency coefficient in goodness-of-fit measures for daily runoff simulation with SWAT. *J Hydrol Eng* 22(11):1–9
- Lindzen RS, Nigam S (1987) On the role of sea surface temperature gradients in forcing low-level winds and convergence in the tropics. *J Atmos Sci* 44(17):2418–2436
- Mann HB (1945) Nonparametric tests against trend. *Econometrica* 13:245–259
- Manwell JF, McGowan JG, Rogers AL (2010) *Wind energy explained: theory, design and application*, 2nd edn. Wiley, UK, p 705
- McPhaden MJ, Meyers G, Ando K, Masumoto Y, Murty VSN, Ravichandran M, Syamsudin F, Vialard J, Yu L, Yu W (2009) RAMA: the research moored array for African–Asian–Australian monsoon analysis and prediction. *Bull Am Meteorol Soc* 90(4):459–480
- McVicar TR, Donohue L, Jianguo VN, Thomas T, Paul G, Jurgen J, Deepak H, Youcef M, Natalie MK, Andries DY (2012) Global review and synthesis of trends in observed terrestrial near-surface wind speeds: implications for evaporation. *J Hydrol* 416–417:182–205. <https://doi.org/10.1016/j.jhydrol.2011.10.024>
- Mohan S, Bhaskaran PK (2019a) Evaluation and bias correction of global climate models in the CMIP5 over the Indian Ocean Region. *Environ Monit Assess* 191:806. <https://doi.org/10.1007/s10661-019-7700-0>
- Mohan S, Bhaskaran PK (2019b) Evaluation of CMIP5 climate model projections for surface wind speed over the Indian Ocean Region. *Clim Dyn* 53(9–10):5415–5435. <https://doi.org/10.1007/s00382-019-04874-2>
- Moriiasi DN, Arnold JG, Van Liew MW, Bingner RL, Harmel RD, Veith TL (2007) Model evaluation guidelines for systematic quantification of accuracy in watershed simulations. *Trans ASABE* 50(3):885–900. <https://doi.org/10.13031/2013.23153>
- Morim J, Hemer M, Andutta F, Shimura T, Cartwright N (2020) Skill and uncertainty in surface wind fields from general circulation models: intercomparison of bias between AGCM, AOGCM and ESM global simulations. *Int J Climatol* 40(5):2659–2673
- Muthige M, Malherbe J, Engelbrecht F, Grab S, Beraki A, Maisha TR, Merwe JVD (2018) Projected changes in tropical cyclones over the South West Indian Ocean under different extents of global warming. *Environ Res Lett*. <https://doi.org/10.1088/1748-9326/abc60>
- Nagababu G, Kachhwaha SS, Naidu NK, Savsani V (2017) Application of reanalysis data to estimate offshore wind potential in EEZ of India based on marine ecosystem considerations. *Energy* 118:622–631
- Nash JE, Sutcliffe JV (1970) River flow forecasting through conceptual models. Part I—a discussion of principles. *J Hydrol* 27(3):282–290
- Nayak S, Bhaskaran PK, Venkatesan R, Dasgupta S (2013) Modulation of local wind-waves at Kalpakkam from remote forcing effects of Southern Ocean swells. *Ocean Eng* 64:23–35. <https://doi.org/10.1016/j.oceaneng.2013.02.010>
- Parvathi V, Suresh I, Lengaigne M, Izumo T, Vialard J (2017) Robust projected weakening of winter monsoon winds over the Arabian sea under climate change. *Geophys Res Lett* 44(19):9833–9843
- Parvathy KG, Bhaskaran PK (2019) Nearshore modelling of wind-waves and its attenuation characteristics over a mud dominated shelf in the Head Bay of Bengal. *Reg Stud Mar Sci*. <https://doi.org/10.1016/j.rsma.2019.100665>
- Patra A, Bhaskaran PK (2016) Trends in Wind-wave climate over the head Bay of Bengal region. *Int J Climatol* 36(13):4222–4240
- Patra A, Bhaskaran PK (2017) Temporal variability in wind-wave climate and its validation with ESSO-NIOT wave atlas for the head Bay of Bengal. *Clim Dyn* 49(4):1271–1288
- Patra A, Bhaskaran PK, Jose F (2018) Time evolution of atmospheric parameters and their influence on sea level pressure over the head Bay of Bengal. *Clim Dyn* 50(11–12):4583–4598
- Rahaman H, Srinivasu U, Panickal S, Durgadoo JV, Griffies SM, Ravichandran M, Bozec A, Cherchi A, Voldoire A, Sidorenko D, Chassignet EP, Danabasoglu G, Tsujino H, Getzlaff K, Ilıcak M, Bentsen M, Long MC, Fogli PG, Farneti R, Danilov S, Marsland SJ, Valcke S, Yeager SG, Wang Q (2020) An assessment of the Indian Ocean mean state and seasonal cycle in a suite of interannual CORE-II simulations. *Ocean Model* 145:101503
- Rani SI, Das Gupta M, Sharma P, Prasad VS (2014) Intercomparison of Oceansat-2 and ASCAT winds with in situ Buoy observations and short-term numerical forecasts. *Atmos Ocean* 52(1):92–102. <https://doi.org/10.1080/07055900.2013.869191>
- Reguero BG, Menéndez M, Méndez FJ, Mínguez R, Losada IJ (2012) A global ocean wave (GOW) calibrated reanalysis from 1948 onwards. *Coast Eng* 65:38–55
- Rehman S (2013) Long-term wind speed analysis and detection of its trends using Mann–Kendall test and linear regression method. *Arab J Sci Eng* 38(2):421–437
- Ritter A, Muñoz-Carpena R (2013) Performance evaluation of hydrological models: statistical significance for reducing subjectivity in goodness-of-fit assessments. *J Hydrol* 480(1):33–45. <https://doi.org/10.1016/j.jhydrol.2012.12.004>
- Roxy MK, Ritika K, Terray P, Masson S (2014) The curious case of Indian Ocean warming. *J Clim* 27(22):8501–8509
- Sahoo B, Bhaskaran PK (2016) Assessment on historical cyclone tracks in the Bay of Bengal, East Coast of India. *Int J Climatol* 36(1):95–109
- Sandhya KG, Bala Krishnan Nair TM, Bhaskaran PK, Sabique L, Arun N, Jaykumar K (2013) Wave forecasting system for operational use and its validation at coastal Puducherry, East Coast of India. *Ocean Eng* 80:64–72. <https://doi.org/10.1016/j.oceaneng.2014.01.009>
- Semedo A, Sušelj K, Rutgersson A, Sterl A (2011) A global view on the wind sea and swell climate and variability from ERA-40. *J Clim* 24(5):1461–1479
- Semedo A, Weisse R, Behrens A, Sterl A, Bengtsson L, Günther H (2013) Projection of global wave climate change toward the end of the twenty-first century. *J Clim* 26:8269–8288. <https://doi.org/10.1175/JCLI-D-12-00658.1>
- Sempreviva AM, Furevik B, Cheruy F, Barthelmie RJ, Jimenez B, Tranteric C (2006) Estimating off-shore wind climatology in the Mediterranean area, comparison of QuikSCAT data with other methodologies. *OWEMES 2006*, 20–22 April, Civitavecchia, Italy
- Shanas PR, Sanil Kumar V (2015) Trends in surface wind speed and significant wave height as revealed by ERA-interim wind wave Hindcast in the Central Bay of Bengal. *Int J Climatol* 35(9):2654–2663
- Simmons AJ, Berrisford P, Dee DP, Hersbach H, Hirahara S, Thépaut JN (2017) A reassessment of temperature variations and trends from global reanalyses and monthly surface climatological datasets. *Q J R Meteorol Soc* 143(702):101–119

- Sinha M, Jha S, Chakraborty P (2020) Indian Ocean wind speed variability and global teleconnection patterns. *Oceanologia* 62(2):126–138. <https://doi.org/10.1016/j.oceano.2019.10.002>
- Sreelakshmi S, Bhaskaran PK (2020) Spatio-temporal distribution and variability of high threshold wind speed and significant wave height for the Indian Ocean. *Pure Appl Geophys*. <https://doi.org/10.1007/s00024-020-02462-8>
- Srivastava A, Dwivedi S, Mishra AK (2016) Intercomparison of high-resolution Bay of Bengal circulation models forced with different winds. *Mar Geod* 39(3–4):271–289
- Stouffer RJ, Eyring V, Meehl GA, Bony S, Senior C, Stevens B, Taylor KE (2017) CMIP5 scientific gaps and recommendations for CMIP6. *Bull Am Meteorol Soc* 98(1):95–105
- Swapna P, Krishnan R, Wallace JM (2014) Indian Ocean and monsoon coupled interactions in a warming environment. *Clim Dyn* 42:2439–2454. <https://doi.org/10.1007/s00382-013-1787-8>
- Taylor KE (2001) Summarizing multiple aspects of model performance in a single diagram. *J Geophys Res Atmos* 106(D7):7183–7192
- Tokinaga H, Xie SP (2011) Wave- and anemometer-based sea surface wind (WASWind) for climate change analysis. *J Clim* 24(1):267–285
- Vandemark D, Vachon PW, Chapron B (1998) Assessment of ERS-1 SAR wind-speed estimates using an airborne altimeter. *Earth Obs Q* 59:5–8
- Wang XL, Feng Y, Swail VR (2014) Change in global ocean wave heights as projected using multimodel CMIP5 simulations. *Geophys Res Lett* 41:1026–1034. <https://doi.org/10.1002/2013GL058650>
- Wentz FJ, Ricciardulli L, Hilburn K, Mears C (2007) How much more rain will global warming bring? *Science* 317(5835):233–235
- Willmott CJ, Ackleson SG, Davis RE, Feddema JJ, Klink KM, Legates DR, O'Donnell J, Rowe CM (1985) Statistics for the evaluation and comparison of models. *J Geophys Res* 90(C5):8995–9005
- Young IR, Ribal A (2019) Multiplatform evaluation of global trends in wind speed and wave height. *Science* 364(6440):548–552
- Young IR, Zieger S, Babanin AV (2011) Global trends in wind speed and wave height. *Science* 332(6028):451–455. <https://doi.org/10.1126/science.1197219>
- Zhang X, Vincent LA, Hogg WD, Niitsoo A (2000) Temperature and precipitation trends in Canada during the 20th century. *Atmos Ocean* 38(3):395–429
- Zou T, Kaminski ML (2014) Predictions of climate change impact on fatigue assessment of offshore floating structures. Delft: Department of Maritime and Transport Technology, Delft University of Technology, p 10

Publisher's Note Springer Nature remains neutral with regard to jurisdictional claims in published maps and institutional affiliations.